2013

Silver (Ag) nanoparticle based masks for the development of antireflection subwavelength structures in GaAs and Si solar cells

Nazme A. Moushumy
Edith Cowan University

Edith Cowan University

Copyright Warning

Silver (Ag) Nanoparticle Based Masks for the Development of Antireflection Subwavelength Structures in GaAs and Si Solar Cells

By

Nazme Ara Moushumy

A thesis submitted in fulfilment of the requirements for the degree of Master of Engineering Science

At

Electron Science Research Institute

Faculty of Computing, Health and Science

EDITH COWAN UNIVERSITY

Supervisors:

Prof. Kamal Alameh & Dr. Mikhail Vasiliev

December 2013

USE OF THESIS

The Use of Thesis statement is not included in this version of the thesis.

DECLARATION

I certify that this thesis does not, to the best of my knowledge and belief:

(i) Incorporate without acknowledgement any material previously submitted for a degree or diploma in any institution of higher education;

(ii) Contain any material previously published or written by another person except where due reference is made in the text; or

(iii) Contain any defamatory material.

I also grant permission for the Library at Edith Cowan University to make duplicate copies of my thesis as required.

Date: 4th of December 2013

ACKNOWLEDGEMENTS

First and foremost, I am grateful to The Almighty God for enabling me to complete my thesis successfully.

I dedicate this thesis to my deceased father and mother, who brought me in this world.

I would like to express my sincere gratitude to my principal advisor Prof. Kamal Alameh for the continuous support of my research, for his patience, motivation, enthusiasm, and immense knowledge. His guidance and can-do attitude helped throughout my research and writing of this thesis.

I would also like to gratefully and sincerely thank my co-supervisor Dr. Mikhail Vasiliev for his support on lab experiment and thesis writing. His intellectual guidance and invaluable comments keep on the right path during my study and thesis writing.

I am thankful to my former co-supervisor N. Das for his continuous support during the initial days. I also like to thank all of my friends and colleagues for their help. I like to thank ECU Graduate school for giving me an opportunity of my Masters study .I take this opportunity to record my sincere thanks to Mrs. Linda Arthur, Mrs. Tiella Turkovic and Mr. Paul Roach for all their administrative support.

My deepest gratitude goes to my Husband Sajedul Khan for his unflagging love and support throughout my study. He has been a true and great supporter and has unconditionally helped me during my bad and good times. I owe my loving thanks to my son, Labib and daughter Lamia, who have been the most valuable gift in my life.

Finally, I would like to thank my spiritual teacher Shahid Al Bokhari, whose direction about life brought me in this lively life and has given me the inspiration to enjoy my journey in this world. As a result, I have completed my thesis smoothly.

PUBLICATIONS

1. Nazme Moushumy, Kamal Alameh, V. Rajendran and Yong Tak Lee, **"**Silver-Nanoparticle-Based Etch Mask Control for Subwavelength Structure Development", Nanosystems: Physics, Chemistry, Mathematics, 4(3),Page(s): 387-394, St. Petersburg National Research University of Information Technologies, Mechanics and Optics, 2013.

2. Nazme Moushumy, Kamal Alameh, V. Rajendran, and Yong Tak Lee, "Silver nanoparticle size and spacing control for low-reflectivity structure development", Proceedings of 6th International Symposium on Macro and Super molecular Architectures and Materials (MAM-2012), Coimbatore, India, page(s):219-224, November 2012.

3. Nazme Moushumy, N. Das, Kamal Alameh and Yong Tak Lee; "Design and Development of silver nanoparticles to reduce the reflection loss of solar cells", High capacity Optical Networks and Enabling Technologies (HONET), Riyadh, page(s): 38-41, 2011.

ABSTRACT

This thesis focuses on the design and development of silver nanoparticles that can be used as masks for the development of antireflection subwavelength grating (SWG) structures. We particularly investigate the impact of silver thin film thickness and the effect of annealing temperature on the fabrication of silver nanoparticles of controlled size and spacing distributions. We also use these measured distributions to predict the performance of subwavelength grating structures developed using dry and isotropic etching of semiconductor substrates.

Silver (Ag) thin films of different thicknesses are deposited on Silicon (Si) and Gallium Arsenide (GaAs) semiconductor substrates and annealed at different temperatures. Uniform nanoparticles with diameters around 200nm and spacing between nanoparticles as low as possible are our target as these parameters are suitable for the fabrication of antireflection SWG structures, having grating widths equal to the nanoparticle diameter and spacing equals to the spacing between nanoparticles. Experimental results demonstrate that by annealing the Ag thin films with different temperature profiles, it is feasible to develop Ag nanoparticles, of diameter around 200nm and spacing below 250nm, at most of the annealing temperatures investigated.

In addition, different subwavelength structures, developed by etching the Ag nanoparticles deposited on Si and GaAs substrates, are simulated using a Finite-Difference Time Domain (FDTD) software package. The simulation results show that substantial reduction in light reflection can be achieved by optimizing the height of the subwavelength structures through the control of the etching time.

CONTENTS

LIST OF TABLES

LIST OF FIGURES

Chapter 1

Introduction

The conversion efficiency of many types of solar cell structures critically depends on the reflectivity of their top surfaces. For Silicon (Si) and Gallium Arsenide (GaAs) semiconductor solar cells, the average reflectivity of the top surface is more than 27%, depending on their refractive index over the solar spectrum. Traditionally, to lower the surface reflectivity (thus increase the conversion efficiency) of the solar cells, antireflection (AR) thin film coatings have been used. However, the use of thin-film coatings has various disadvantages, including, (i) complex deposition processes which require expensive vacuum deposition equipment, (ii) lower yield due to the addition of a thin film deposition process, and (iii) mechanically unstable performance under high-temperature operation.

Subwavelength grating (SWG) structures are an alternative to optical coatings which has long been demonstrated and used for bulk optical surfaces [1, 2]. Typically, SWG structure has a small pitch that enables the suppression of all diffraction orders, except the 0^{th} order, thus allowing minimum light reflection, and hence, maximum light transmission.

Subwavelength grating (SWG) structures have recently attracted enormous interest over the last decade particularly in the field of photovoltaics as they have several interesting advantages. For example, integrating an SWG onto a solar cell device provides almost a lossless reflecting surface that enhances the solar cell's efficiency [3].

The SWG often takes a one- and/or two-dimensional periodic configuration. If the pitch (or period) of a single grating structure is less than the wavelength of the incident light, it behaves like a homogeneous medium with an effective refractive index [4]. So, SWG structures enable gradual changes in the refractive index, thus assuring an excellent antireflective medium together with a light trapping phenomena in comparison to planar thin films [1,4]. A nanorod structure acts as a single layer antireflective (AR) coating, while the triangular (conical) and parabolic shaped grating structures are more advantageous since they behave like a multilayer broadband AR coating [4].

In this thesis, we report on the control of silver nanoparticle size and spacing for the development of low reflectivity structures. Silver nanoparticles are fabricated by Ag thin film deposition in conjunction with thermal annealing, and subsequently, conical shaped SWG structures are realized through the etching of Silicon (Si) and Gallium Arsenide (GaAs) substrates onto which the developed silver nanoparticles are deposited.

In order to understand the effects of Ag thin-film thickness and annealing temperature on the size and spacing of the Ag nanoparticles, several silver (Ag) thin films of thicknesses 10nm, 8nm and 5nm are deposited on GaAs and Si substrates and annealed at different temperatures leading to the development of randomly distributed Ag nanoparticles on the surface of each sample. Different nanoparticle diameters and spacing between nanoparticles are achieved by controlling annealing temperature and film thickness, which give rise to SWG structures having different grating widths and spacings. Finite Difference Time Domain (FDTD) simulation of these SWG structures confirms the low reflection in comparison with flat substrates.

The thesis is organised as follows: Chapter 2 is a literature review describing solar cell operation, types of photovoltaic cells, photovoltaic energy conversion efficiency, antireflection coatings for solar cell and SWG structures, basic mechanism of antireflection coatings, moth-eye structures, subwavelength grating structures (SWG), nanoparticles and their applications, simulation of light propagation through SWG structure. Chapter 3 focuses on the design and fabrication of nanoparticle arrays. In Chapter 4 we discuss the techniques used to characterise the fabricated nanoparticle arrays. In Chapter 5 we report on the fabrication of silver nanoparticles using thin film deposition in conjunction with thermal annealing, and predict the performance of conical shaped SWG structures realised through the etching of Si and GaAs substrates whereon the developed silver nanoparticles are deposited.

Chapter 2

Literature review

2.1 Solar Cells:-

2.1.1 Solar Cell Operation:-

Solar cells convert light energy into electrical energy either by converting it into heat, or through a direct process known as photovoltaic effect. A potential difference or voltage is produced when light strikes a two-layer semiconductor material. The voltage produced can pass a current through an external electrical circuit that can be utilized to power electrical devices. This is the basic concept of solar cell operation.

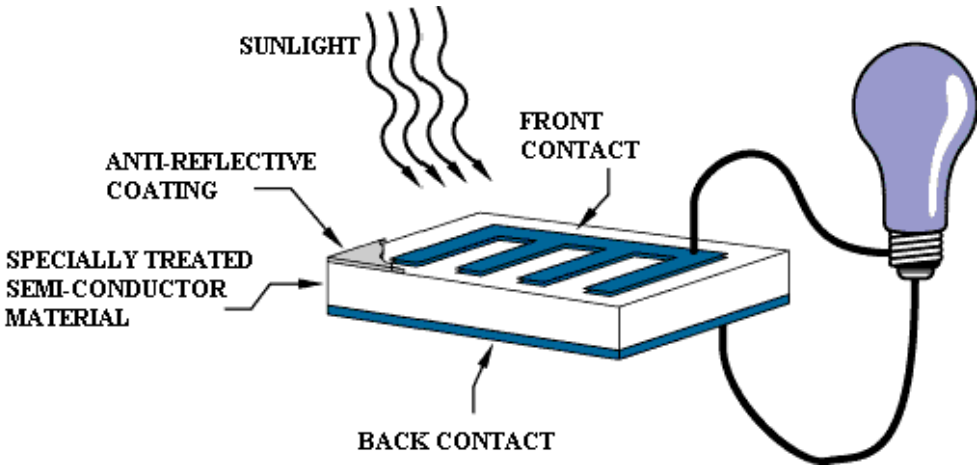

Fig.2.1: Basic diagram of a solar cell (source 5).

Fig. 2.1 illustrates the operation of a basic solar cell. A specially treated semiconductor material is used to generate an electric field, with a positive charge on one electrode and a negative charge on the other. When energy is added to the semiconductor, electrons are freed from their bonds. By applying a metal contact

layer to both sides of the semiconductor, as shown in figure 2.1, and providing an electric circuit, free electrons can be captured and flow, generating electricity [6].

When sufficient energy (for example, heat) is added to pure silicon, some electrons are freed from their crystal bond structure and create a hole and can move randomly, as well as searching for other holes in order to combine with them by releasing excess energy. These free electrons are capable of producing current when in the presence of an external circuit. As there are very few free electrons in pure silicon, the level of current would be insignificant. The free electrons or holes can be increased by adding some impurities. Phosphorus (P) and boron (B) are commonly used as impurities. The process of adding impurities is called doping. In phosphorus, five electrons are in the outer shell, so when added as a dopant to silicon four electrons of phosphorus form bonds with the outer shell electrons of the silicon atom (Fig. 2.2). The fifth valence electron cannot form a bond; so a small amount of energy is able to move the electron away from the crystal structure. Because of the free electrons in phosphorus–doped silicon, it is called N-type silicon (N standing for negative). In Fig. 2.3 P-type silicon, there are three valance electrons in the outer shell of boron. These three electrons form a bond with three outer shell electrons of silicon but the fourth electron of silicon has no electron to bond with. The absence of an electron in the crystal lattice creates a hole and these holes act as positive charges by attracting electrons. The boron-doped silicon is called P-type silicon (P standing for positive).

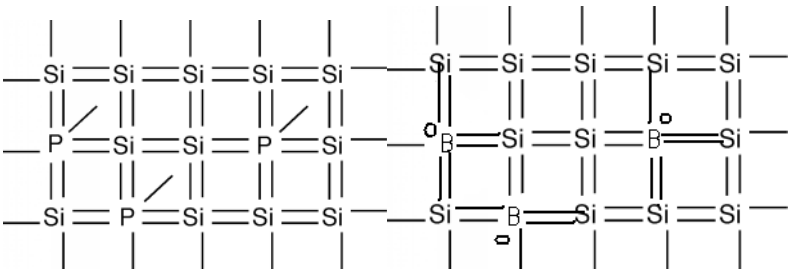

Free electron

Fig. 2.2 N-type silicon.

Hole

Fig. 2.3 P-type silicon.

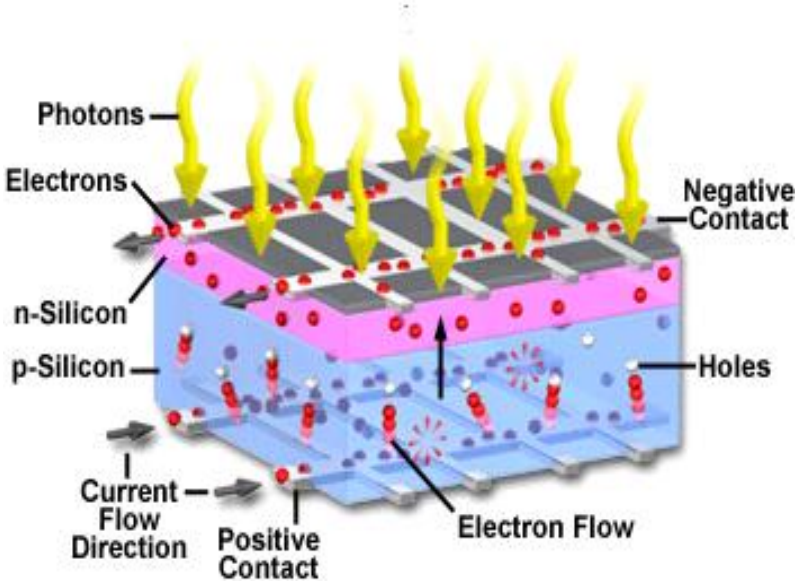

Fig. 2.4: Electron and current flow in solar cell [source 6].

In a typical photovoltaic cell, two layers of doped silicon semiconductor are tightly bonded together (as shown in Fig. 2.4). One layer is modified to have excess free electrons (N-type), while the other layer is treated to have an excess of electron holes (P-layer). When the two dissimilar semiconductor layers are joined at a same boundary, the free electrons in the n-layer cross into the p-layer to fill the electron holes. The electrons and holes at the p-n junction create a barrier that hardly allows additional electrons to cross. Across the boundary a fixed electric field results, as the electrical imbalance reaches an equilibrium condition which separate the two sides P-layer and n-layer[6].

The electrons can move randomly in the presence of particular wavelengths of light. The electrons near the boundary (P-N junction) can be swept out and enter into the N- junction creating a charge imbalance between the two layers. The electrons cannot return to the p-region against the field gradient but have a tendency to return to neutralize the charge imbalance. In this situation, an external circuit that connects the two semiconductors creates an alternate path, allowing the electrons to return to P-region from N-region, which produces a current flow. Metal contact layers are applied to the outer faces of the two semiconductor layers in the construction of a photovoltaic cell and are connected by an external circuit.

2.1.2 Types of Photovoltaic Cells:-

There are three types of solar cell commonly used:

i) Mono-crystalline (single crystal)

Mono-crystalline solar cells are produced from pure silicon. Pure silicon is produced by applying high temperature to silicon dioxide and carbon in a reduction reaction.

The governing chemical reaction is:

$$SiO_2 + C \rightarrow Si + CO_2$$

A controlled amount of boron, an impurity, is added in the molten silicon. A "seed" crystal of silicon is then drawn out of melt. A regular crystal structure depends upon the temperature of the molten silicon and the speed at which the "seed" crystal is withdrawn. The crystal structure of silicon is tetrahedral in shape, with each silicon atom bonded to four other silicon atoms. The crystal is then sliced into wafers. Silicon doped with phosphorous joins together with the boron doped silicon wafer.

Metal contacts are applied to both the front and back surface of the wafer enabling it to produce electricity, thereby creating a "solar cell" [7].

ii) Poly-crystalline (Many crystals)

Many tiny crystals forced together at random make a block of silicon and this is called poly-crystalline silicon. The block is sliced, doped and contacts applied in the same way as for mono-crystalline cells. It is generally cheaper and requires less energy to produce than mono-crystalline cells [7].

iii) Amorphous (no specific crystal structure)

Condensation of gaseous silicon deposits a thin film of silicon directly onto a backing surface and the atoms in this thin film are arranged in a completely random fashion. The cell is called an amorphous thin-film cell [7].

2.1.3 Photovoltaic Energy Conversion Efficiency:-

There are several factors which influence the efficiency of solar cells. The following main factors limit the efficiency for mono-crystalline cells [7]:

- ***Crystal Structure of silicon*:-**

  - Mono crystalline solar cells have a well defined cell structure and there is very little chance of reverse current flow across the depletion layer. Their efficiency is up to 23% in laboratory conditions.
  - In polycrystalline solar cells the efficiency is about 6% less than the mono-crystalline solar cells.
  - Amorphous cells, with no crystal structure, have a much lower efficiency, typically about 6% when new and this efficiency drops away as the cell ages.

- ***How tightly the cells are packed to form a module:-***

  There are small gaps between neighbouring cells when cells are connected together to form modules. No electricity is produced by solar radiation falling on these gaps.

- ***Metallic contact area :***

  There is metallic contact in a solar cell which is connected by an external circuit. This metallic contact is essential to produce electricity but it prohibits some incoming solar radiation.

- ***Quantum factors***

  Some of the incoming photons of solar radiation do not strike electrons at all. Some photons strike the electron but don't have sufficient energy to eject the electron. Some photons have excess energy, much of which may be wasted as heat, and some photons strike impurity atoms or the nuclei of silicon atoms. All these factors reduce solar cell efficiency.

- ***Reflection loss***

  Some of the incoming solar radiation is reflected from the surface of the cell and never gets the chance to eject an electron.

Temperature and radiation intensity are two other factors that affect solar cell efficiency.

2.2 Antireflection coatings for solar cell and SWG structures:-

The optical reflectivity of a surface can be reduced by using an antireflection (AR) coating that covers a certain wavelength range. The AR coating is normally a dielectric thin film applied to the optical surface.

The first antireflection coatings were made by Joseph Fraunhofer in 1817 [8]. After one year, Augustin Jean Fresnel developed a different theory based on Thomas Tong and Christiaan Huygens. James Clerk Maxwell published his treatise on electromagnetism 56 years before. In 1954, the first practical solar cell was announced and it did not employ any ARCs. It was later discovered that ARCs were necessary to increase the efficiency of solar cells by reducing reflection loss [8].

2.2.1 Basic mechanism of antireflection coatings:-

Efficiency of a solar cell can be increased by using an anti-reflection coating that reduces reflection in certain wavelengths (IR, Visible UV gives good performance). The basic principle of operation is that reflected waves from different optical interfaces largely cancel out each other by destructive interference. Minimum reflectance can be achieved when the refractive index equates to the square root of the refractive index of two medium [1]. The strength of the reflection depends on the refractive index of the two medium and the angle of the surface to the beam of light.

Fig. 2.5 shows the reflection and transmission of a glass substrate with a thin film coating. In this figure, light is travelling from air into a common glass substrate. The intensity of the incident light is I, reflected light is R.I and transmitted light is T.I. If a thin film coating is applied to the glass substrate, it reduces the reflection. Here, I is the incident light on the coating, R_{01} is the reflected light at the interface of air and thin film coating, and the transmitted light is $T_{01}I$. The incident light at the coating and glass interface is $T_{01}I$, the transmitted light is $T_{1s}T_{01}I$ and the reflected light is $R_{1s}T_{01}I$.

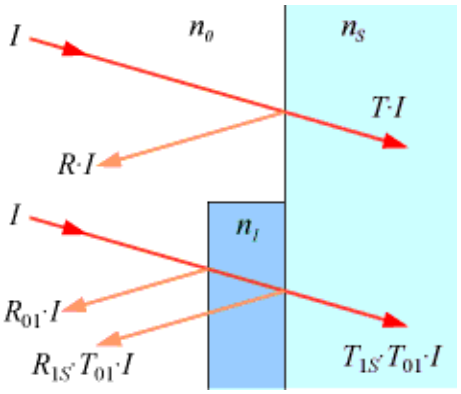

Fig 2.5 Reflectance of a glass substrate is reduced using a thin film (source 9).

The percentage of reflection can be calculated by the well-known Fresnel equations [9]:

$$R = \left(\frac{n_0 - n_s}{n_0 + n_s} \right)^2 \quad \text{..... (1)}$$

where, R = Reflection coefficient or reflectance.

n_0 = refractive index of the first media

$n_{s=}$ refractive index of the second media

If visible light travelling from air (n_0 = 1.0)into common glass (n_s = 1.5), the value of R is therefore 4%.If a thin film is applied tothe glass surface, it reduces the reflection loss. The optimum refractive index $n_1 = \sqrt{(n_0 n_s)}$

= 1.225

For this refractive index, the reflection loss of each interface, R = 1%. i.e., the total reflection loss = 2%.

Therefore, an intermediate coating between the air and glass can reduce the reflection loss to half (about 50%).

It is important to note that the greater the number of coating layers in an ARC arrangement, the lower the average reflectance becomes, provided the materials are chosen such that they are close to the optimal refractive index. For multilayer coatings, the refractive index is;

$\boldsymbol{n_m = n_{sup}^{\left(\frac{M+1-m}{M+1}\right)} n_{sub}^{\left(\frac{m}{M+1}\right)}}$ [source 10]..... (2)

where n_m is the refractive index of the m^{th} layer out of M layers,

n_{sub} is the refractive index of the substrate and n_{sup} is the refractive index of the superstrate [10].

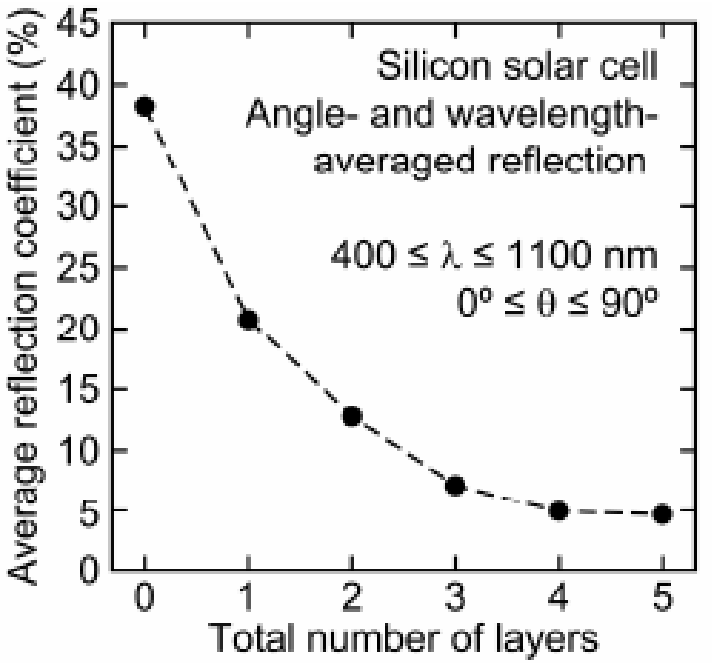

Fig. 2.6: Reflection coefficient (i.e. % of light reflected), angle- and wavelength-averaged reflection, as a function of the number of layers for optimized ARCs for silicon solar cells(Source11).

From Fig. 2.6, it is obvious that the percentage of light reflected decreases with increased numbers of layers. However, formation of multilayer coating film can be a complex process and there are some drawbacks, such as adhesion and thermal mismatch and instability under thermal cycling [1,3].

2.2.2 Moth-eye structures:-

Standard antireflection coating works within a limited range of wavelengths and incident angles of sunlight (angles between the light rays and the cell's surface). This angle of incidence continuously changes throughout the day making it difficult to

absorb optimum amounts of sunlight. Recently, the moth's eye concept is being used in solar cells to reduce reflection. Moth's eye reflects very little amount of light at night due to its arrayed nanopillars that collectively behave as an intermediate refractive index at the air-medium interface. This structure works as an antireflective coating for a broad range of wavelengths and for any incident angle of light. The antireflective behaviour of moth's eye nanostructures is necessary for solar cells that aim to collect broad spectrum sunlight at continuously changing incident angles. The nano-structured film consists of a hexagonal pattern bump which is 200nm high. This acts as an antireflective coating because the bumps are smaller than the wavelength of visible light. The refractive index between the air and the surface changes gradually, thus decreases the reflection at the surface. [12,13].

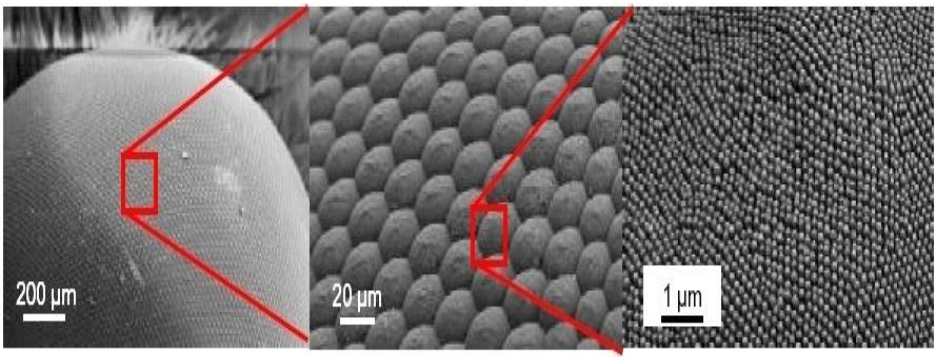

Fig. 2.7 Moth-eye structure (Source 13).

2.2.3 Subwavelength grating structures (SWG):-

Subwavelength grating structures can be formed by lithography, colloidal formation, nano-imprint and nano-particles etc. [13]. These types of structures can minimise reflection but lithographic techniques such as electron beam lithography, nano-imprint lithography and interference lithography require sophisticated equipment and are expensive to implement [14]. Any "roughening" of the surface reduces reflection

by increasing the chances of reflected light bouncing back onto the surface, rather than out into the surrounding air.

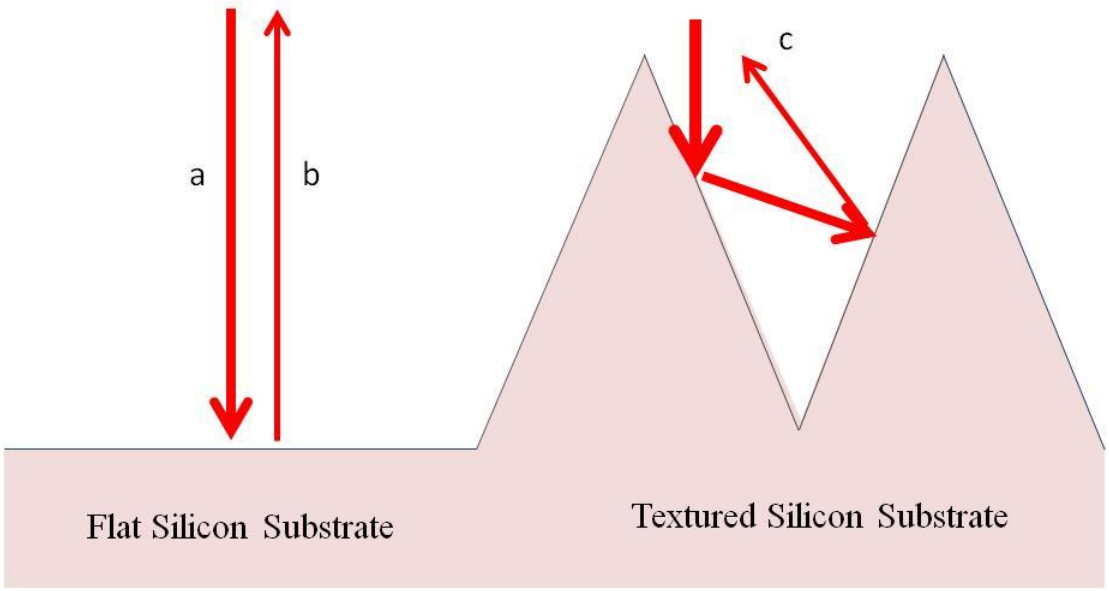

Fig. 2.8 Light reflection phenomena for flat silicon substrate and textured silicon substrate.

In Fig. 2.8, (a) Incoming light, strikes a surface with reflection R, (b) The reflected light from the surface is reflected at the same angle at which the incoming light strikes the surface, (c) In a textured surface, rather than being lost, the reflected light can strike the silicon surface again thus reducing the reflection.

In silicon solar cells, surface texturing is being used as a reflection-reducing technique and combining it with ARCs has been a standard feature since the mid-1970s [15]. In the most general sense, texturing involves roughening the silicon surface to scatter or redirect light.

Sub-wavelength features cause a gradual change in refractive index which acts as a multilayer antireflection coating leading to low reflection over broadband ranges of wavelength and angle of incidence. Fig. 2.9 shows a gradual change of a grating structure as well as refractive index leading to low reflection. A nanorod structure

acts as a single layer antireflective coating whereas a triangular shaped grating structure acts as a multilayer antireflective coating [13].

If we consider Fig. 2.9 and try to evaluate the reflection according to Fresnell's equation, we can easily see that reflection is reduced in every situation other than the flat substrate.

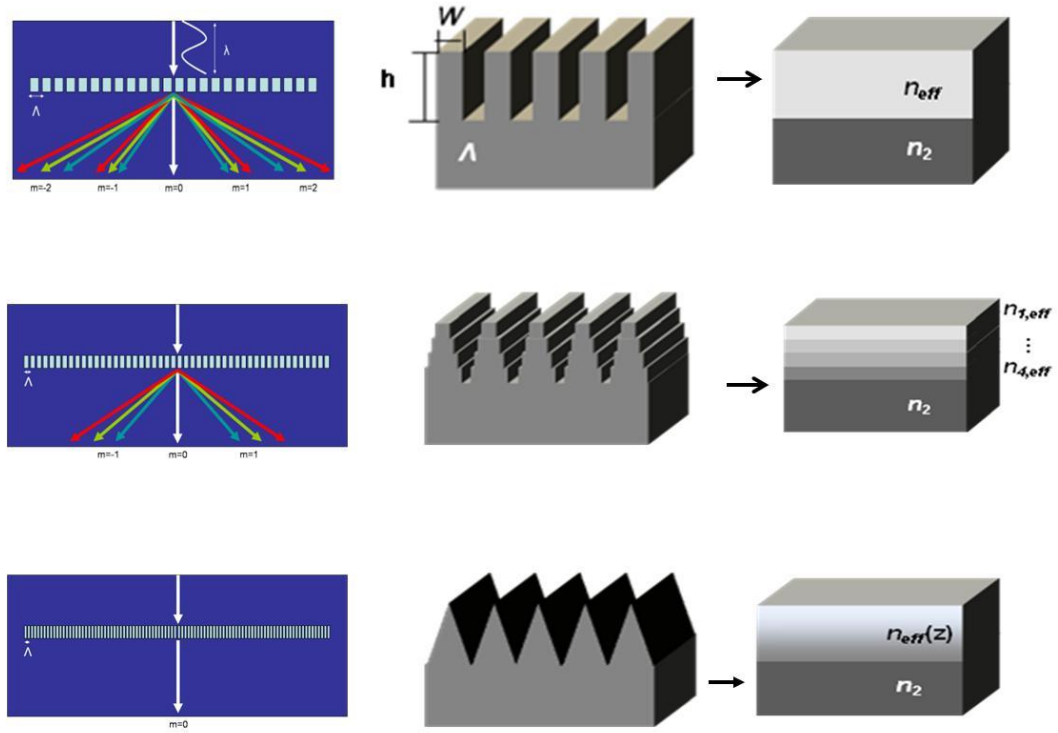

Fig. 2.9 Reflection of rectangular and triangular (conical) shaped SWG structures (source 13).

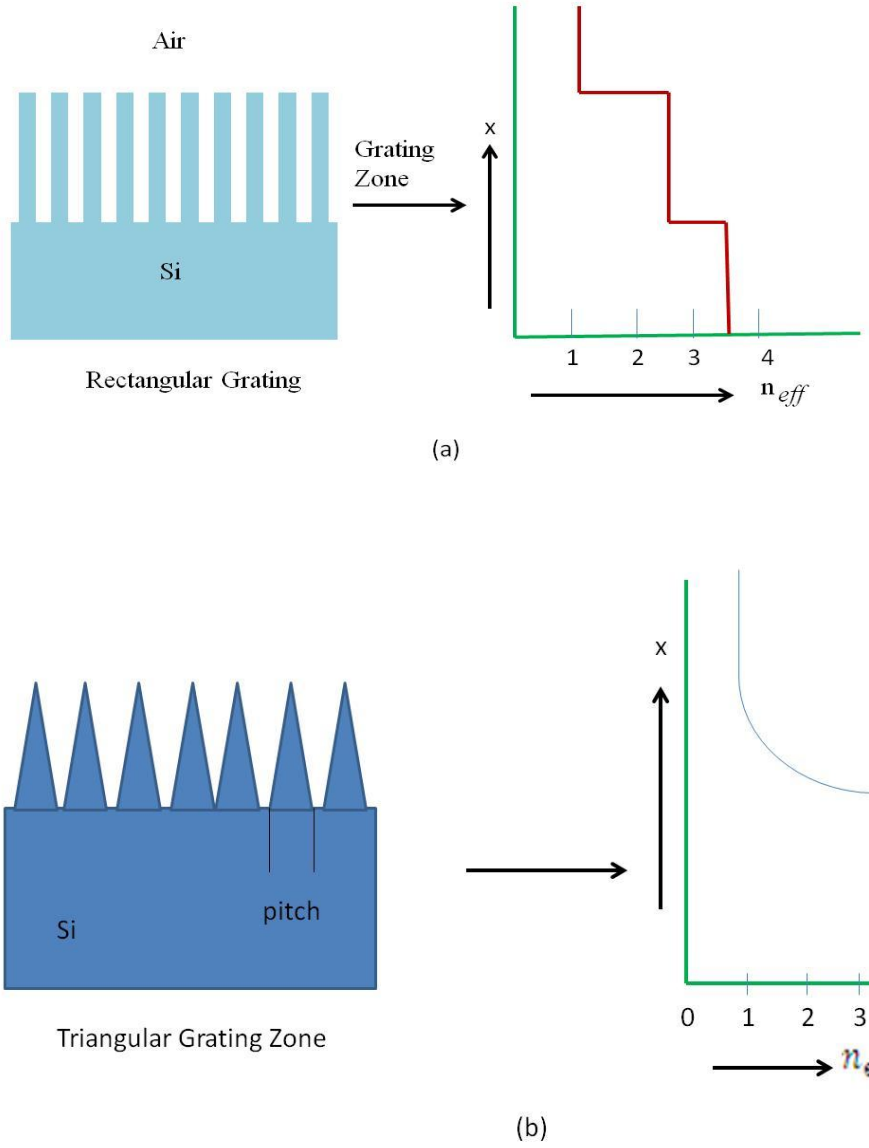

Fig. 2.10 Refractive index profile of (a) rectangular and (b) triangular (conical) shaped SWG structures on a Si-air interface.

In a rectangular-shaped SWG structure, the refractive index changes very sharply from air (n = 1) to the grating zone or structure (approximately 2.5) [1]. The reflection loss of an SWG structure can be calculated easily using Fresnell's equation:

$$R = \left(\frac{n_2 - n_1}{n_2 + n_1} \right)^2 \quad \text{..... (3)}$$

where, n_1 is the refractive index of first medium and n_2 is the refractive index of second medium.

From Fig. 2.10, we can calculate the total reflection of the grating structure using the following equation:

$R_{tot} = R_1 + R_2$ ..……(4)

where, R_1 is the reflection at the interface of air and grating structure and R_2 is the reflection at the interface of the grating structure and substrate.

If the grating structure has a shorter pitch (or period) than the wavelength of the incident light, it acts as a homogeneous medium with an effective refractive index. Fig. 2.10 (a) shows a rectangular shaped grating structure where the refractive index decreases sharply from air to the grating zone and again decreases from the grating zone to the silicon substrate leading to less reflection. In the triangular (conical) shaped SWG structure, the refractive index changes gradually i.e it acts as a multilayer grating structure that lowers reflection than the rectangular grating structure. In this paper, the reflection loss was calculated using Opti-FDTD software package developed by Optiwave Inc.

The first–order expressions for the refractive index are also calculated by the following equation [1]:

$n_{parallel} = \{f n_1^2 + (1-f) n_2^2\}^{1/2}$ .....(5a)

$n_{perpendicular} = \left(\frac{f}{n_1^2} + \frac{(1-f)}{n_2^2} \right)^{-1/2}$ ..... (5b)

Equation (5a) and (5b) refer to the case of the electric field of the incident light being parallel or perpendicular to the grooves respectively (TM and TE respectively).

Where, n_1 = refractive index of the first medium

n_2 = refractive index of the second medium

f = filling factor

For triangular gratings, the fill factor profile is a linearly decreasing function along the depth of the grating (i.e., f=1/h where h is the depth of the grating). For rectangular gratings, the resulting effective profile is equivalent to that of single layer coating. The effective refractive index can be controlled by changing the duty cycle of SWG. Therefore, according to the thin film theory,

Film refractive index $n_f^{AR} = \sqrt{n_1 n_2}$

The advantage of SWGs solar cell is that the cell efficiency is sustained over 60°C incident angle and it is degraded only 8 % at 70°C. So, most of the day, light can be absorbed and provide a solar cell with better efficiency [13].

2.3 Nanoparticles and their applications:-

Nanoparticles are a promising area of scientific interest due to a wide variety of potential applications in optical, electronic and biomedical fields. The small portion of a particle in nanoscale size is called nanoparticles. The synthesis, characterization and exploration are described in nanoscience and nanotechnology. The physical and chemical properties of nanoparticles can differ significantly from the bulk materials of the same composition. The principal parameters of nanoparticles are their shape, size and morphological sub structure of the substance. Suitable control of these properties and response of nanostructures can lead to new devices and technologies [16].

Most nanoparticles are made of noble metals or non-reactive metals such as gold, silver and sometimes aluminium, copper or zinc. The nanoparticles can be formed and often stabilized by having charged particles attracted to the surface of the nanoparticles.

Fig. 2.11 shows the dynamic behaviour of Ag nanoparticles on surfaces. Most notably, under ambient conditions at relative humidity greater than 50%, new Ag nanoparticles are formed in the vicinity of the parent particles [17].

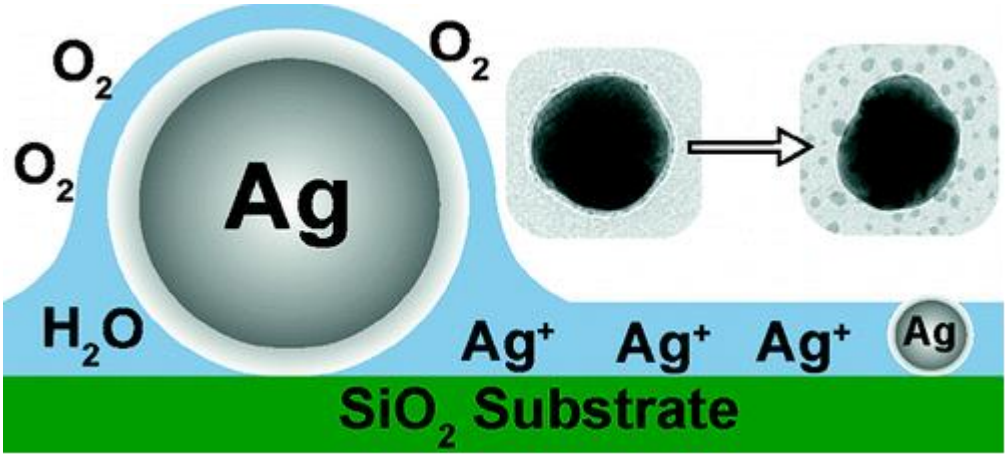

Fig. 2.11 Silver nanoparticles formation on a silica(SiO_2) substrate (source 17).

Nanoparticles formation occurs through a three stage process: (1) oxidation and dissolution of silver from the surface of the particle, (2) diffusion of silver ion across the surface in an absorbed water layer, and (3) formation of new, smaller particles by chemical and/or photoreduction.

Silver nanoparticles are great significant as different properties such as magnetic, optical and electrical are dependent on the size. Silver nanoparticles have contributed to many scientific areas of research, such as electronics, optics, catalysts, water treatment, textile engineering, bioengineering, biotechnology, medical devices etc. [18, 19].

2.4 Simulation of light propagation through SWG structure:-

Opti-FDTD software is user-friendly, powerful and highly integrated allowing computer aided design and simulation of advanced passive photonic components. The software package is based on the finite difference time domain method. The FDTD method is an established powerful engineering tool for integrated and diffractive optics device simulations due to its unique combination of features, such as the ability to simulate light propagation, scattering and diffraction, reflection and polarization effects. This method is applicable for the effective and powerful simulation and analysis of sub-micron devices with very fine structural details.

The first step in the simulation process is the Opti-FDTD layout design. Opti-FDTD comes as 4 main applications: i) Layout designer: Here we need to define the structure and simulation conditions, ii) Profile designer: The materials and profiles used in the simulation is defined here, iii) Simulator: The designer file is loaded in this program and performs the simulation, and iv) Analyzer: this program performs some post processing and is used to view the results. After completion of the simulation, the simulator will ask if we would like to open the analyzer.

Fig. 2.12 is a flow chart that illustrates the main steps for building a layout.

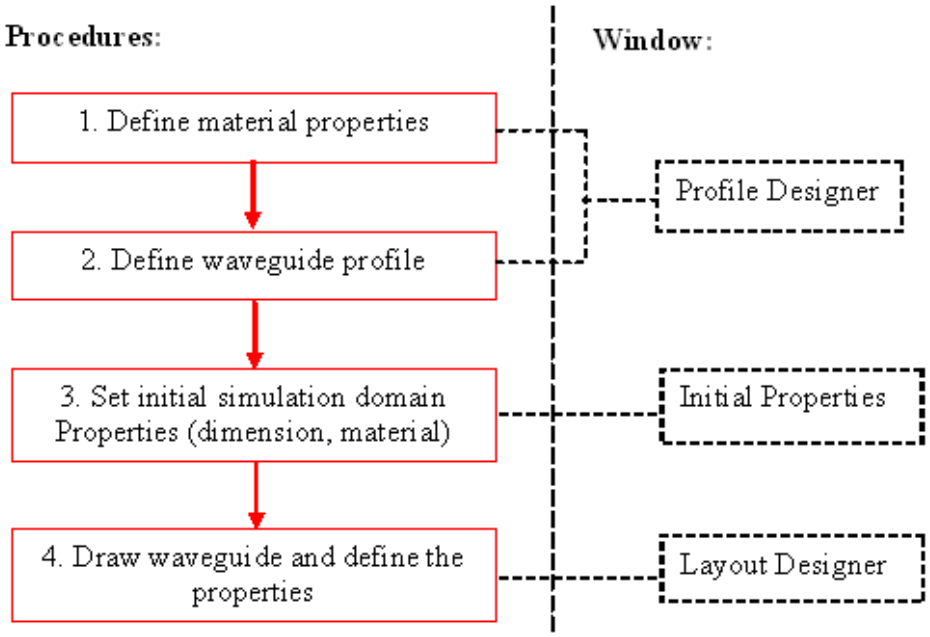

Fig. 2.12 Flowchart for building a layout in Opti-FDTD software (source 20).

The simulation domain can be 2D, that is a finite XZ-area, or 3D, that is XYZ volume. For 3D simulation the domain is divided into 2 parts called substrates and cladding. The design concept is illustrated in Fig. 2.13. There is a channel waveguide consisting of two rectangular layers, it is suspended in the cladding volume and extends along the Z directions. A fibre waveguide consisting of two circular fibre layers is imbedded in the substrate and also extends along Z-direction. The cross section of the rectangular waveguide and the fibre is called a profile.

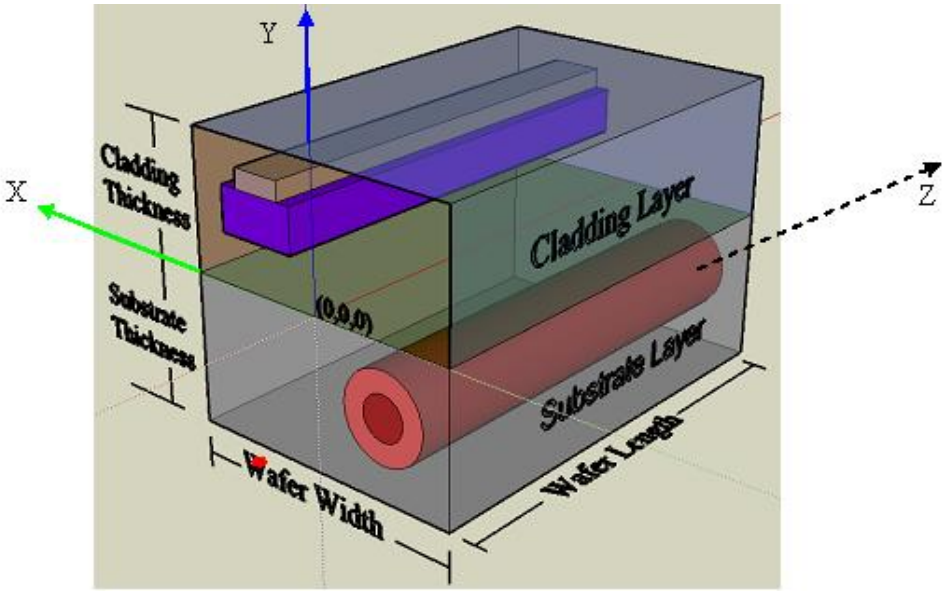

Fig. 2.13 Project layout illustrating the design concept of Opti-FDTD software (Source 20).

For simulation of light reflection, the source of light is designed above the substrate. When the design is completed, simulation can start. In all simulation activities undertaken, 2D simulation was adequate for accurately predicting the reflectance of investigated SWG structures. When the Simulator starts, the emitting field can be observed as shown Fig. 2.14.

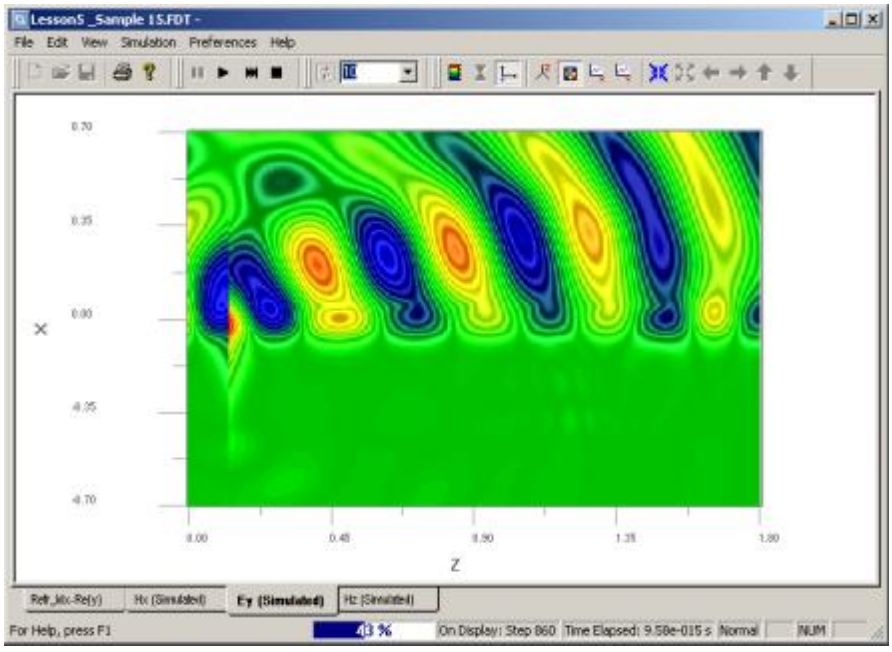

Fig. 2.14 Schematic diagram of a simulation process (Source 20).

When the simulation ends, a message appears and asks to open Opti-FDTD Analyzer. Through the analyzer, we can observe the result. Here we observe a line graph of reflection against wavelengths of light.

Chapter 3

Design and fabrication of metal nanoparticle arrays

Metal nanoparticles have been of interest for more than a century because of their chemical and physical property. These properties are being utilized in various research fields. In our experiment, Ag nanoparticles are fabricated for use as a mask in the SWG fabrication process. By controlling the size, shape and spacing of the nanoparticles, we are able to synthesis SWG structures with suitable parameters of low reflection. Wet colloid chemistry, metal thermal deposition or lithographic techniques are some of the popular methods for the fabrication of nanoparticles. Optical nanolithographic techniques are widely used and known by different names depending on the exposure source. The key elements of a standard photolithographic system are a set of masks, an energy source and a medium. Optical lithographic systems require the same key elements [4].

Electron beam lithography is adequate for very small diameter nanoparticles [3] but it is relatively expensive. Our target was to fabricate nanoparticles with around 200nm diameter giving low reflection. X-ray lithography is another good method but it is also expensive [21]. Nanosphere lithography is good as it can fabricate nanoparticles having controlled size, shape and spacing and allow for large area fabrication, and is relatively simple and inexpensive but suitable for making particle sizes upto 100nm[22]. Metal deposition by thermal evaporation is one of the oldest, cheapest and simplest methods and can be used in large area production.

In this Chapter we describe the RF magnetron sputtering processing, which is based on physical vapour deposition, and especially used for the deposition of Ag thin film,

and the subsequent high-temperature annealing process necessary to develop Ag nanoparticles with a desired average diameter.

3.1 Sputtering Deposition Processes:-

RF magnetron sputtering is a widely used method, based on physical vapour deposition for the fabrication of high quality films at low operating pressure. The substrate and target material are placed inside the system as shown in Figure 3.1, as attached to the anode and cathode of the sputtering system, respectively. A weakly charged gas of particles (called a plasma) is created by ionizing a sputtering gas (generally a chemically inert, heavy gas like Argon).Since ions are charged particles, electric and magnetic fields can control the velocity and energy of the ions. When ions collide with surface atoms on the target, the energy transfer knocks some of these atoms off the target's surface.

The target atoms/molecules traverse the vacuum chamber and condense on the substrates resulting in the desired thin film being deposited onto the substrate.

(a)

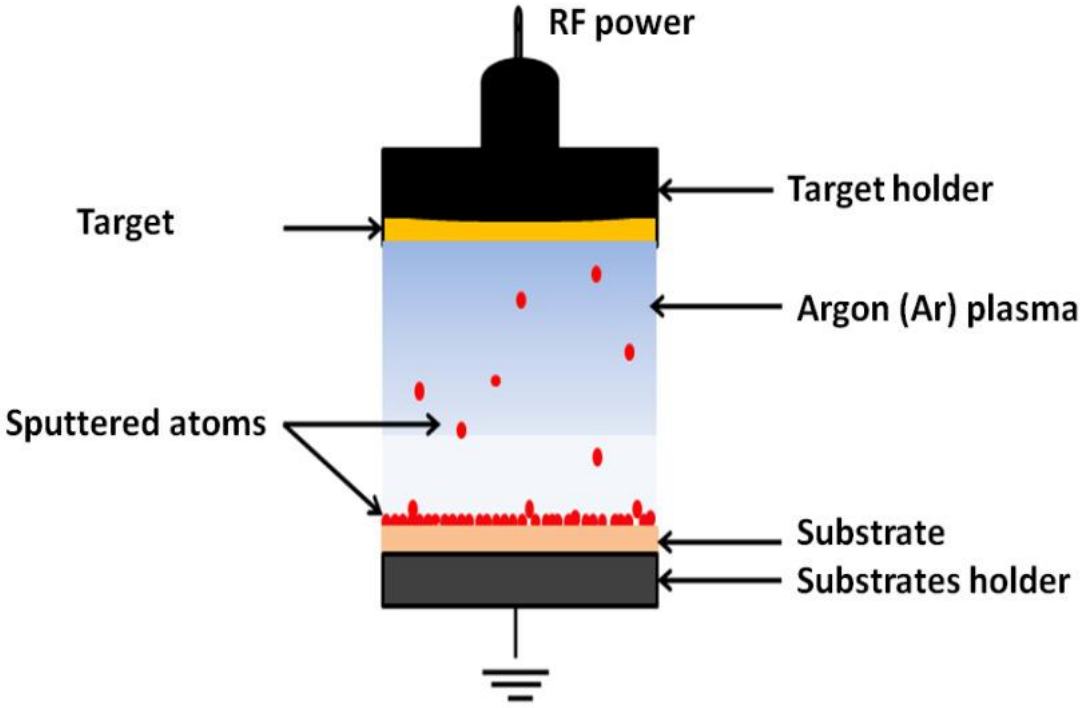

(b)

Fig. 3.1 (a) Photograph of the RF magnetron sputtering system used for the deposition of metal thin films. (b) Schematic diagram of the sputtering process.

The RF magnetron system shown in the Fig. 3.1 was used to prepare Ag thin films on Si and GaAs substrates. 10nm, 8nm and 5nm Ag thin films on Si and GaAs were deposited. The thickness of each film was monitored during the sputtering process with in-situ reflectometry system. During the thin film deposition an s-polarized light was impinged on the middle of the substrate and the thickness of the growing film was measured by capturing the reflected power with the detector using "Real-Time Thickness Control for Multilayers" software made at ECU [23].

3.2 Annealing and nanoparticle formation from thin metallic layers:-

A heat treatment process wherein a material is modified, causing changes in its properties such as strength and hardness is called annealing. In this process conditions are produced by heating the substrate to above the re-crystallization temperature and then cooling it. Annealing is used to soften material, actuate

ductility, relieve internal stresses, modify the structure by making it homogeneous and improve cold working properties. In the case of Ag thin film annealing, this process is performed by substantially heating the thin film, generally until glowing, and then allowing it to cool slowly in air or quickly by quenching in water. Through heating, the metal is softened and prepared for further processing such as shaping or stamping [24,25].

Heat supplies energy to a solid material, thus increasing its diffusion rate and progressing it towards its equilibrium state. The movement of atoms has the effect of redistributing and destroying the dislocations in metals. This alternation in dislocations increases their ductility. The amount of Gibbs free energy that is needed for the initial process is also reduced by the annealing process. This reduction is termed as "stress relief" and it is a spontaneous process but at room temperature it is a very slow process [24,25].

A conventional temperature ramp-controlled box furnace oven was used in our experiment to fabricate nanoparticles. Fig. 3.2 shows that annealing that was carried out through three steps:

i) Heating the sample to the recommended temperature where temperature ramp-up process is used;

ii) Keeping the temperature constant for a definite time period which is called isothermal crystallization; and

iii) Cooling the substrate at the same temperature ramp rate.

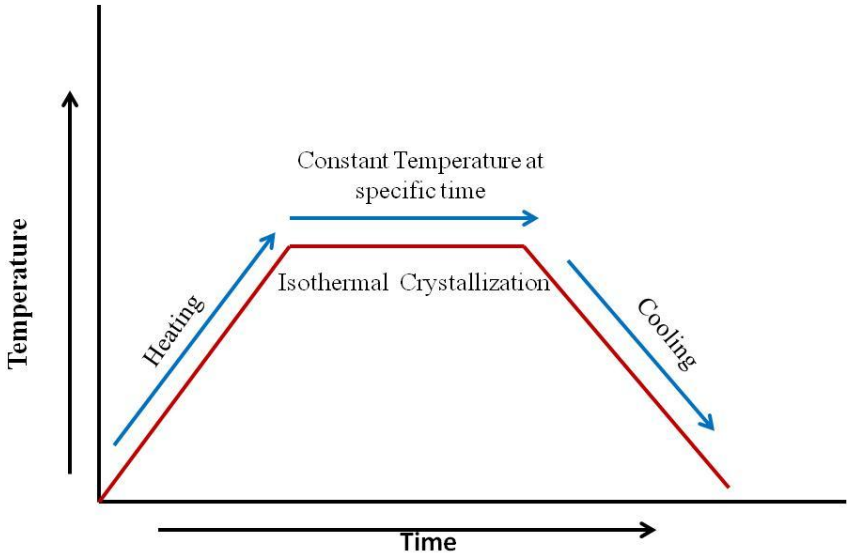

Fig. 3.2 Schematic diagram of the annealing process used to fabricate Ag nanoparticles on Si and GaAs substrates with the conventional box-furnace-type oven annealing system.

In our experiment different thicknesses Ag on Si and GaAs samples were annealed at temperature range 523K to 723K, at temperature ramp 5°C/min and isothermal phase fixed at 30 minutes. We observed that the annealing temperature and metal film thickness can be used to control the average particle size and distance between the nearest metal nanoparticles.

3.3 Formation of subwavelength grating structures:-

There are several conventional methods for the fabrication of conical SWG structures, such as photolithography, colloidal formation, nanoimprint and nanoparticles. Unfortunately, perfect conical shapes cannot be obtained by any of these methods. The formation of uniformly distributed nanoparticles and the use of dry etching in conjunction with additional isotropic etching processes can produce SWG with almost conical shapes. Fig. 3.3 illustrates the fabrication steps for creating the SWG structure, which were reported by Song et al. [4].

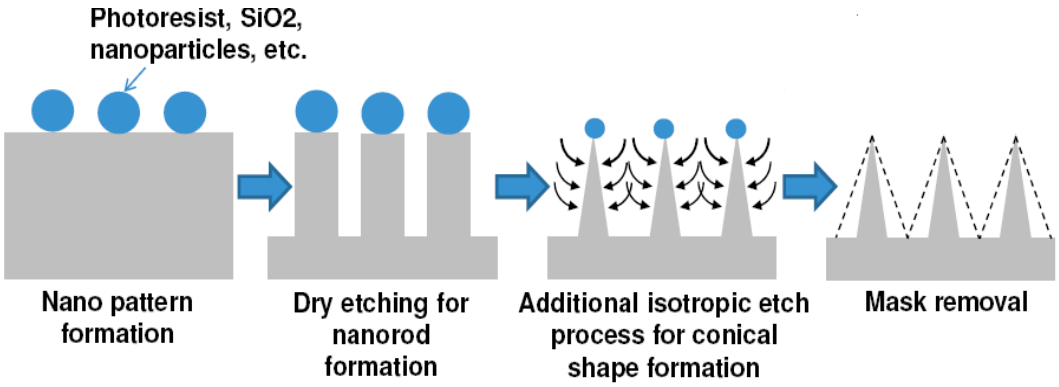

Fig 3.3 Steps for fabricating triangular grating structure [source 13].

At first the nano-particles can be formed using the annealing process, then CF4 or O2 gas is flown through them using dry plasma etching process. To shape the formed nanorods in a perfect conical shape an additional isotropic etching process can be used as reported in [4, 13]. Note that throughout the thesis all Ag nano-particles needed to realize SWG structures were designed, fabricated and characterised at the Electron Science research Institute, ECU.

Chapter 4

Nanoparticle array characterization techniques

Several techniques have been used for detecting, measuring and characterising nanopartricles[26-30].These characterisation techniques include:

- *Transmission Electron Microscopy (TEM)*: This method is particularly useful for measuring the nanoparticle size distribution. In this method an electron beam is used to interact with a sample to form an image on a photographic plate or special camera. The sample needs to be stable under the electron beam and also be able to withstand the high vacuum chamber in which the sample is put. The limitations of this method are the long time consumption and high cost.
- *Atomic Force microscopy (AFM)*: This method is particularly useful for measuring the nanoparticle size and spacing distribution. It is a form of Scanning Probe Microscopy, where a mechanical probe is used to "feel" the surface of a sample. A cantilever with a nanoscale probe is moved over the surface of the sample and from the deflection of the cantilever, the forces between the probe tip and the sample are measured. The deflection moves a laser spot that reflects into an arrangement of photodiodes. This method is suitable for air or liquid samples and is able to measure particle sizes ranging from 1nm to 1µm. It requires less computation time and is less expensive in comparison with TEM.
- *Photon Correlation Spectroscopy (PCS)*: This method is based on dynamic Light Scattering. Average particle size of 1nm to 10µm and size distribution can be measured by this method. However, for this method, the sample must

be a liquid, solution or suspension and must be very dilute otherwise the scattering light can be unclear.

- *Nanoparticle Surface Area Monitoring (NSAM):* This method is mainly used to measure the surface area of nanoparticles that are deposited on a substrate or in a small volume. It can measure the total surface area for particle diameters from 10 nm to 1000 nm. However, this method is typically used in medical applications, where some effects are a function of particle surface area.
- *Condensation Particle Counter (CPC):* The number and concentration of particles are measured by this method. An optical detector is used to enlarge the small particles to a size that can be easily detected. This technique is suitable for aerosol samples and can be used at temperatures as high as 200°C.
- *Differential Mobility Analyzer (DMA)*: The particle size distribution can be calculated by this method, which is based on classifying charged particles according to their mobility in an electric field. A sample is charged and sent into an air flow chamber where an electric field can be applied. Electric mobility can control the rate at which the particles migrate to the end of the chamber. Particles with the same electrical mobility will be the same size; particles can therefore be sorted by size thus the distribution by size is measured.
- *X-ray Diffraction (XRD):* This method is suitable for larger crystalline samples and enables the calculation of the average particle size for bulk samples. Beams of X-rays fall into a sample and the way the beams scatter is

analysed. This method is time consuming and requires a large sample volume for accurate characterisation.

- *Aerosol Time of Flight Mass Spectroscopy*: Particle size and composition of aerosol samples are measured by this method. It is less effective for smaller particle sizes. An aerosol sample is illuminated by a collimated beam of light. The velocities of the particles in the light beam indicates the particle size.
- *Aerosol Particle Mass Analyzer (APM):* This is the only method that gives mass information. It is not dependent on particle size, shape, or orientation of the properties of the gas.
- *Scanning Mobility particle Sizer (SMPS):* It can measure particlesizes ranging from 2.5 nm to 1000 nm. It is based on the use of a continuous, fast-scanning technique to measure high-resolution particle size distribution.
- *Nanoparticle Tracking Analysis (NTA):* This technique can be used to find out the particle size and particle size distribution. A suspension sample is placed on an optically opaque background illuminated by a laser beam. Then the nanoparticles are directly visualised through an optical microscope. A digital camera is typically used to record the observation. A frequency size distribution graph can be obtained by using software. This technique is efficient for 10nm to 1000nm particle sizes.
- *Scanning Electron Microscopy (SEM):* this technique is used for particle size and characterization. Typically, a conductive or sputter coated sample is used and the preparation of the sample is relatively easy, although SEM is a time consuming and expensive method. SEM is capable of measuring particles of diameter down to 1nm. A SEM scans a sample with a focused beam of electrons, which interplay with the atoms of the sample, producing secondary

electrons whose number is a function of the angle between the incident electron beam and the surface. Therefore, scanning of the sample in conjunction with the detection of the secondary electrons produces an image of the sample's surface.

In the characterisation of the developed Ag nanoparticles, we used an in-house SEM which enabled measuring the particle diameter and spacing. Fig.4.1 shows an example of a SEM image of Ag nanoparticles obtained by depositing an 8nm Ag thin film on a GaAs sample and annealing it at 350°C:

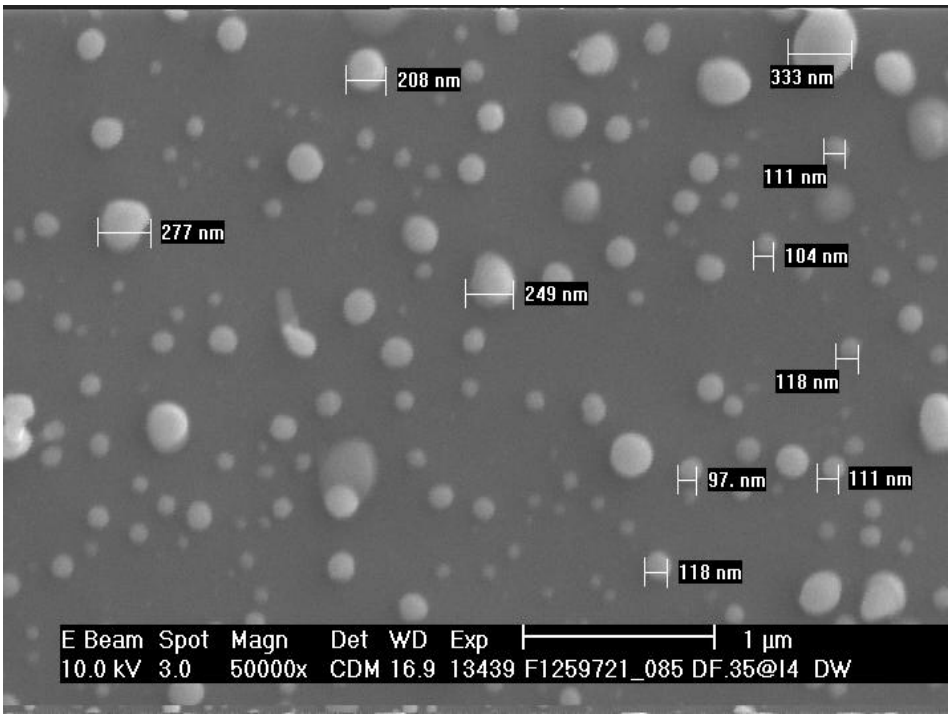

Fig. 4.1 SEM image of Ag nanoparticles obtained by depositing an 8nm Ag thin film on a GaAs sample and annealing it at 623K.

The Ag particle size distribution can be calculated directly from the obtained SEM image, however, this method is time consuming. Instead, ImageJ software, which is a public domain Java processing and analysis program, was used to characterise the developed Ag nanoparticles. This software is typically used to calculate area, pixel value statistics, distance and angles. It can create density histograms and profile plots

and supports standard image processing functions such as contrast manipulation, smoothing, edge detection and median filtering [31]. With the ImageJ software, horizontal straight lines are drawn over the SEM image and the nanoparticle diameter as well as the spacing distributions are automatically generated. 10 lines for each image were adequate for the calculation of the average Ag nanoparticle size and spacing. Fig. 4.2 shows a typical ImageJ plot profile of an annealed Ag sample.

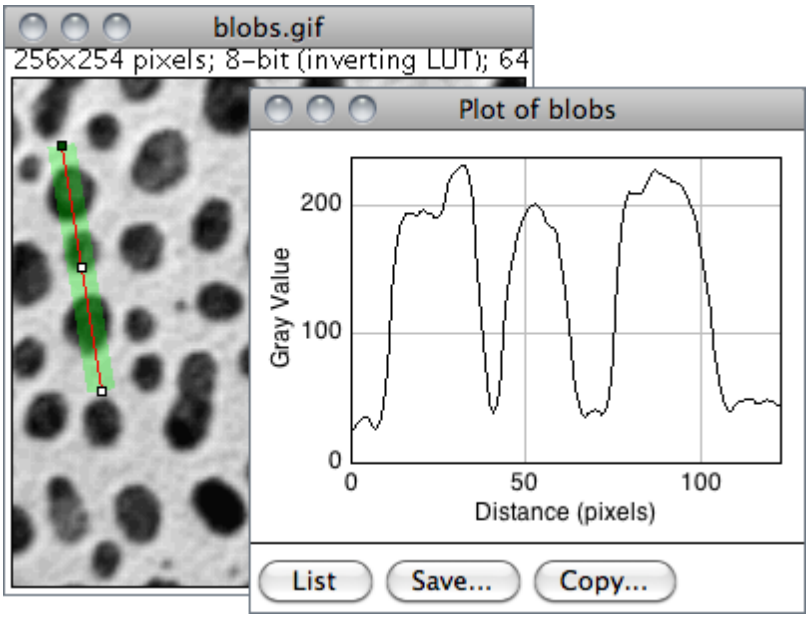

Fig. 4.2 Plot profile of a SEM image.

Fig. 4.2 A two-dimensional graph of the Ag nanoparticle distribution along a line using ImageJ software. In the inset, the x-axis represents the distance along the line and the y-axis is the pixel intensity (Source 31).

Chapter 5

Experimental setups and Results

5.1 Introduction:-

In this chapter, we report on the design and fabrication of silver nanoparticles using thin film deposition in conjunction with thermal annealing, and predict the performance of conical shaped SWG structures realized through the etching of Si and GaAs substrates whereon the developed silver nanoparticles are deposited. Several silver (Ag) thin films of thicknesses 10nm, 8nm and 5nm are deposited on GaAs and Si substrates and annealed at different temperatures ranging from 523K to 723K leading to the development of randomly distributed silver nanoparticles on the surface of each sample. Experimental results show that we can achieve both nanoparticle diameter and spacing close to the desired parameters needed for the fabrication of SWG structures capable of minimizing the reflection loss over the solar spectrum. In addition, the Finite-Difference Time Domain (FDTD) method is used to simulate and optimize the grating height and period size for minimizing the reflection loss of the SWG structure.

5.2 Fabrication of Silver (Ag) Nanoparticle arrays on Gallium Arsenide (GaAs) Substrates:-

To fabricate silver naoparticles, Ag thin films of different thicknesses 10nm, 8nm and 5nm are deposited on GaAs substrates using RF magentron sputtering system and then the deposited samples are annealed in an oven at 523K, 573K, 623K, 673K and 723K for 30 minutes. SEM images of the annealed samples are obtained and characterized by ImageJ software. The annealed samples with their calculated

parameters are then used to design SWG structureswhich can be developed through etching processes. The reflection loss of the SWG structures are simulated by FDTD simulation method and compared with flat substrates.

5.2.1 Ag nanoparticle development:-

Two steps were used for the formation of particle arrays, namely, (i) thin film deposition on GaAs using RF magnetron sputtering system; followed by (ii) annealing of the thin film on GaAs.

(i) *Thin film deposition on GaAs by sputtering method*: Deposition of Ag metal films on GaAs substrates were performed using ESRI's RF magnetron sputtering system described in Chapter 3. The RF magnetron sputtering system is a widely used method, based on physical vapour deposition process that can fabricate high-quality films at low operating pressure. The GaAs substrate, where the target material deposited, was placed inside the vacuum chamber wherein inert Argon (Ar) gas was used as the sputtering gas as shown in Figure 3.1. The argon gas was chosen as the sputtering gas because it does not react with the target material and produces higher sputtering and deposition rates due to its high molecular mass. The target material and the substrate were operating as anode and cathode respectively. An electron beam generated by the electric field accelerated the electrons between the substrate and the target, thus ionise the Ar atoms to Ar^+ ions that sputter target atoms. A permanent magnet located behind the target surface is typically used in the sputtering system in order to maintain plasma confinement and trap electrons thus greatly increases the probability of ionization of the Ar gas within the confinement plasma. Target atoms traverse the vacuum chamber and

condense on the substrates resulting in the desired thin film on the substrate.

Several Ag thin films of thicknesses 10nm, 8nm and 5nm were deposited on GaAs substrates using the RF sputtering system. The film thickness was monitored in real time during the sputtering process using "Real-Time Thickness Control for Multilayers" software made at ECU [23]. The thickness of the growing film was measured by capturing the reflected power using a photodetector in conjunction with an algorithm that can calculate the thin film thickness by comparing the measured the fringe pattern with the modelled one. The operating conditions of the RF magnetron sputtering system at which Ag films on GaAs substrates were deposited are listed in Table 5.1.

Table 5.1

Operating conditions of RF Magnetron Sputtering System for Silver (Ag) thin film deposition on GaAs substrates.

Target	Ag
Substrate	GaAs
Sputtering Gas & Pressure	Argon (Ar), 1-2mTorr
RF Power Density	0.98-1.41
Base Pressure	2-3E^{-06}Torr (High Vacuum)
Substrate surface temperature during deposition process	Room temperature (below 30°C)
Substrate Stage Rotation	32-36rpm
Substrate Target distance	18-20cm

ii) Annealing of thin films on GaAs: The Ag films were then annealed by heating it first then cooling it. As described in Chapter 3, heat provides energy for the materials to break the bonds of atoms and increases the rate of diffusion of the material's atoms during annealing. The diffusion of the material progresses towards its equilibrium state thus redistributing and destroying the

dislocations of the Ag atom sand increasing their ductility. Also, the annealing process reduces the Gibbs-free energy needed for initiating the Ag nanoparticle formation. This reduction is called “stress relief”, which is a spontaneous process at high temperature, but very slow at room temperature [24, 25].

A conventional temperature /ramp-controlled box furnace oven was used in our experiment to fabricate Ag nanoparticles through three steps annealing process which was described in section 3.2.

The annealing process was performed at different temperatures 523K, 573K, 623K, 673K and 723K for a constant time of 30 minutes and the size and distance between the nearest nanoparticles were observed. The aim of this project was to discover (i) the metal film thickness and annealing temperature at which nanoparticles with diameter range around 200nm and spacing between the nearest metal nanoprticles as low as possible can be formed, and (ii) realisation of SWG structures with a grating width and grating distance in the same range of nanoparticle diameter and spacing between nanoparticles that satisfies the condition of less reflection loss.

5.2.2 Characterization of particles and their arrays:-

The images of the annealed samples were taken using Scanning Electron Microscopy (SEM). Particle size and characterization can be observed by this technique. This is a time consuming and expensive method, however sample preparation is easy and the SEM is capable of measuring up to 1nm size particle. The sample is placed under the vacuum and SEM, and should be electrically conductive. In this technique a high energy electron beam is used and the beam is scattered over the surface and subsequently the back scattering of the electrons is observed.

Several samples were placed in the vacuum chamber at the same time and sample images were observed. Fig. 5.1, 5.2 and 5.3 show the SEM images recorded in this experiment:

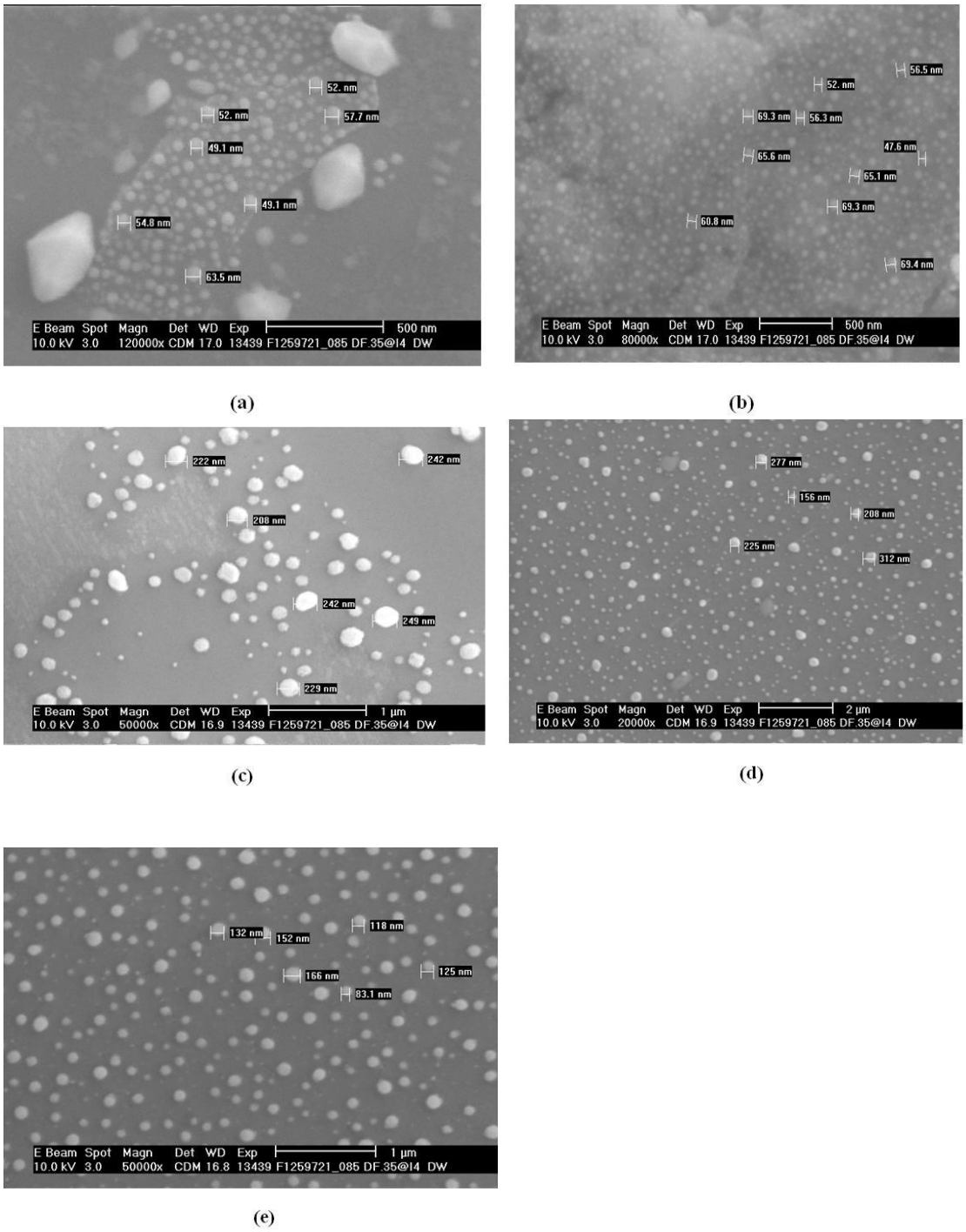

Fig. 5.1 SEM image of Ag nanoparticles obtained by depositing an 5nm Ag thin film on a GaAs sample and annealing at (a) 523K, (b) 573K, (c) 623K, (d) 673K and (e)723K.

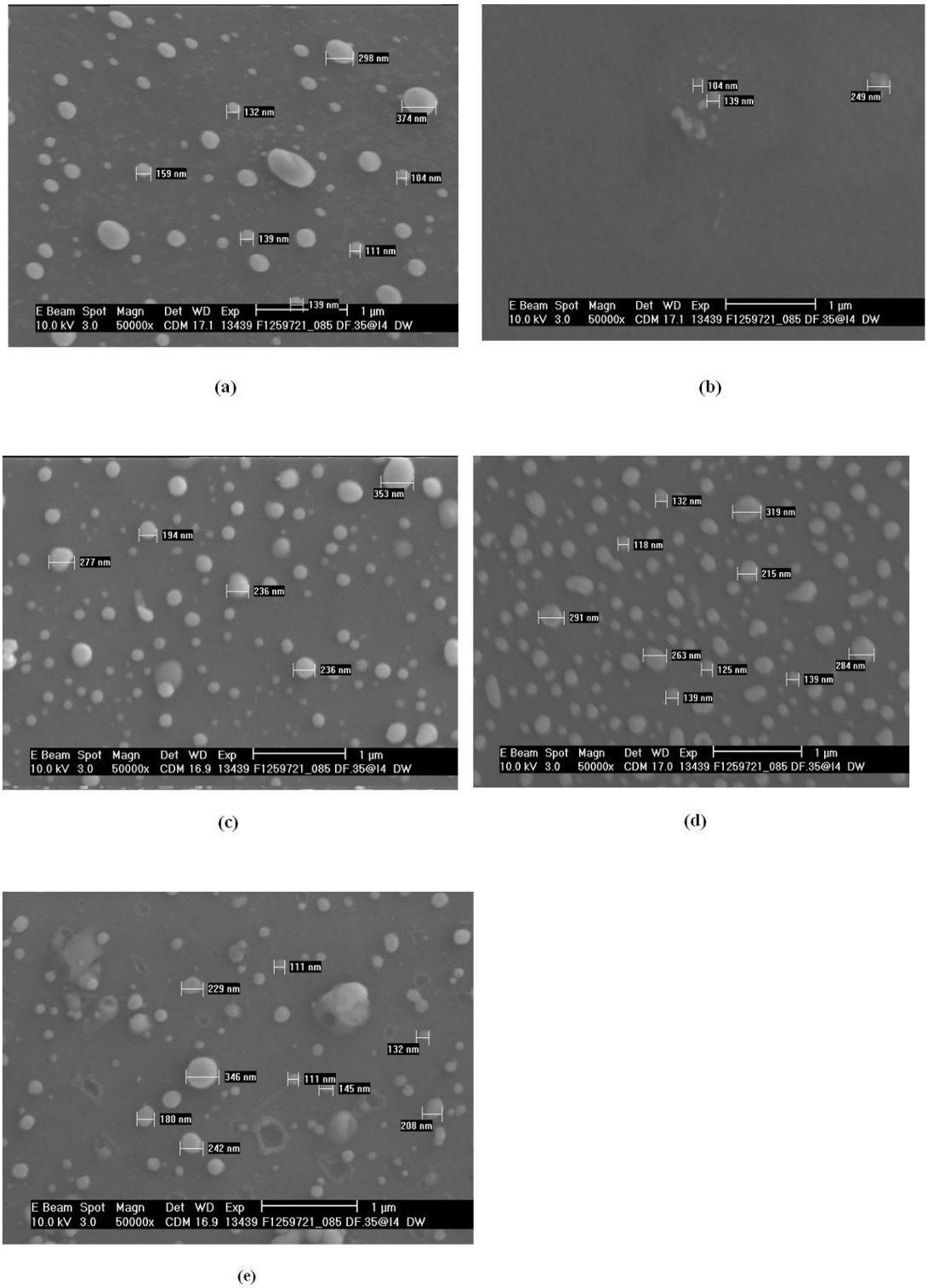

Fig. 5.2 SEM image of Ag nanoparticles obtained by depositing an 8nm Ag thin film on a GaAs sample and annealing at (a) 523K, (b) 573K, (c) 623K, (d) 673K and (e) 723K.

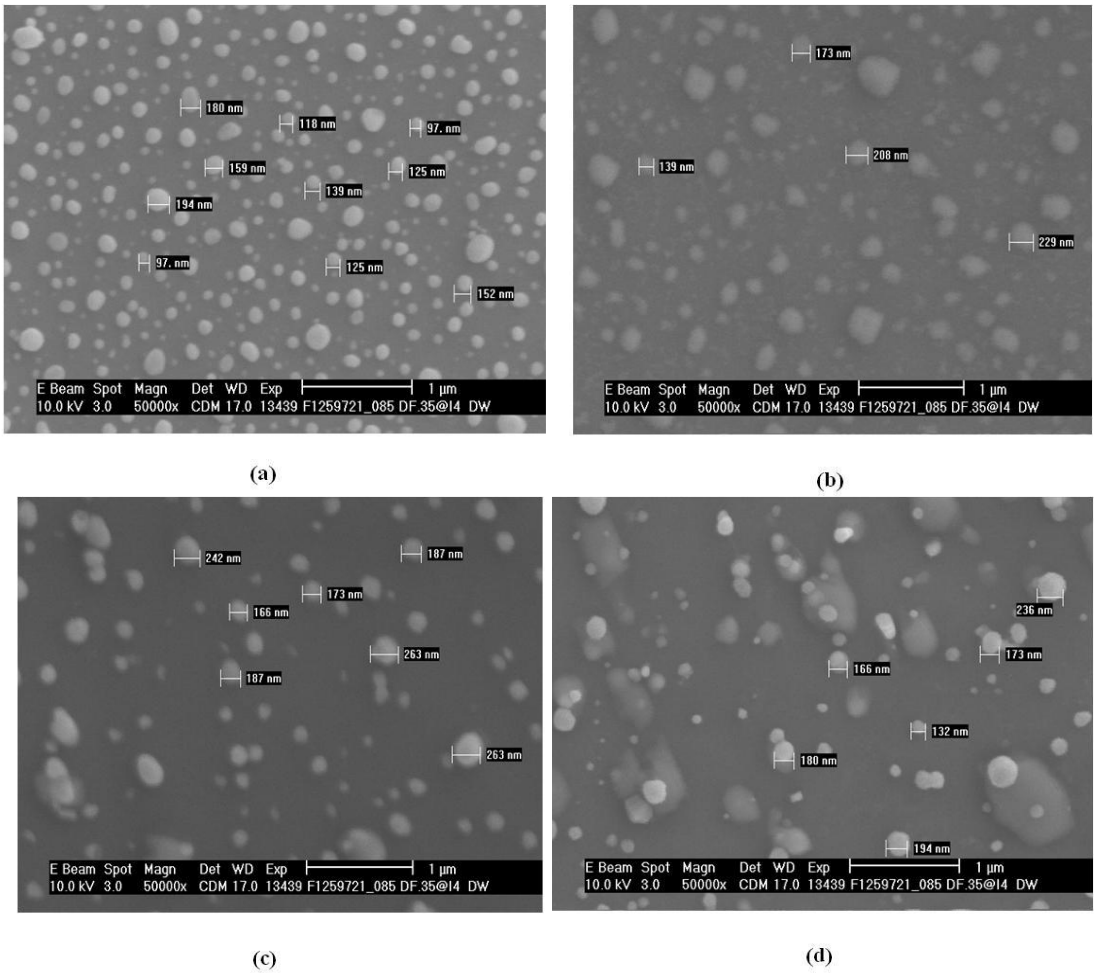

Fig. 5.3 SEM image of Ag nanoparticles obtained by depositing an 10nm Ag thin film on a GaAs sample and annealing at (a) 523K, (b) 573K, (c) 623K and(d) 673K.

We used ImageJ software for calculating the nanoparticle diameter and spacing between nanoparticles. It is a public domain Java processing and analysis program. This software is usually used to calculate area, pixel value statistics, distance and angles. It can create density histograms and profile plots and supports standard image processing functions such as contrast manipulation, smoothing, edge detection and median filtering [31]. In this method we draw a horizontal straight line through the SEM image and measure the nanoparticle diameter and spacing between nanoparticle from the plot profile. 10 lines for each image are drawn and then the average is calculated. Fig. 5.4 shows a plot profile of an annealed sample.

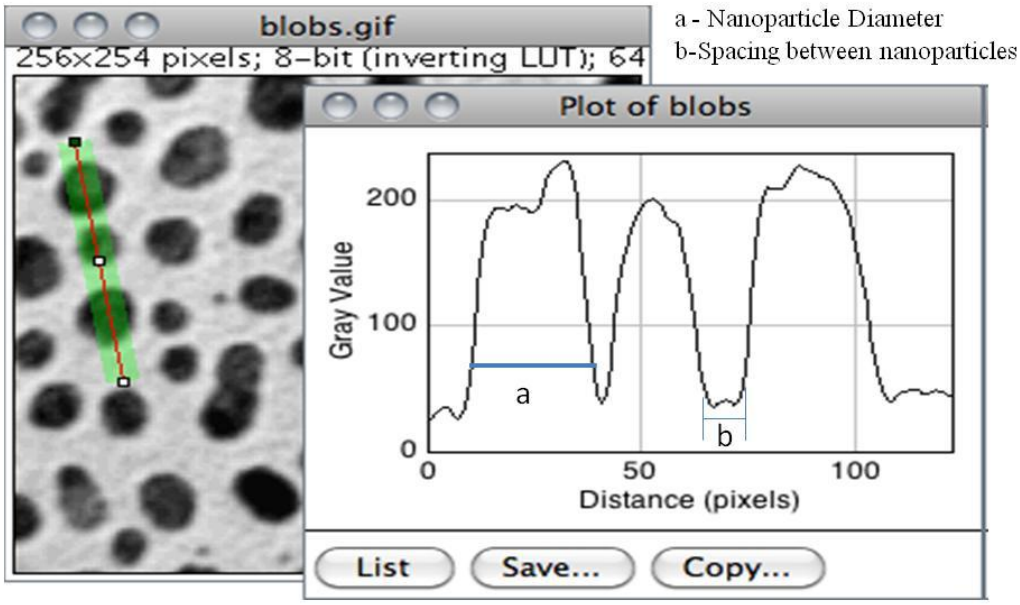

Fig.5.4 Plot profile of a SEM image.

Fig. 5.4 display shows a two-dimensional graph of the intensities of pixels along a line within the image. The X-axis shows distance along the line and the Y-axis is the pixel intensity. For rectangular selections (or line selections wider than one pixel), display a 'column average plot', where the X-axis shows the horizontal distance through the selection and the Y-axis the vertically averaged pixel intensity [31].

5.2.3 Experimental results:-

Nanoparticle diameter and spacing between nanoparticles are calculated by using the above described SEM images and ImageJ software and are listed in Table: 5.2.

Table: 5.2

Different parameters of Ag nanoparticles on Gallium Arsenide (GaAs) substrates

Thickness of Ag film on GaAs substrate(nm)	Annealing Temp.(K)	Diameter of Nanoparticles in nm (Weighted average)	No. of Nanonoparticles	Space between Nanoparticles (nm)
10	523	133	115	302.5
	573	177	78	492.4
	623	180.9	42	953.60
	673	182	44	900
8	523	153	39	867
	623	132.9	56	564
	673	135.7	82	462.9
5	623	158	47	736.4
	673	152.3	120	740.8
	723	126.2	77	567.6

From Table 5.2 it is found that the weighted average diameters obtained through annealing of a 10nm Ag film on GaAs substrate are 133nm, 177nm, 180.9nm, 182nm and average spacing between nanoparticles are 302.5nm, 492.4nm, 953.6nm, 900nm at annealing temperature 523K, 573K, 623K and 673K respectively, for 5nm Ag on GaAs substrate the average diameters are 158nm, 152.3nm, 126.2nm and average spacing between nanoparticles 736.4nm, 740.8nm, 567.6nm at annealing temperature 623K, 673K and 723K respectively and for 8nm Ag on GaAs substrate the average diameters are 153nm, 132.9nm, 135.7nm and average spacing 867nm, 564nm, 462.9nm at annealing temperature 523K, 623K and 673K respectively.

5.2.4. SWG simulation:-

In most practical optical structures, numerical approaches are the only option to evaluating their responses. Fortunately, current computing platforms are fast enough

for modelling complex optical structures within reasonable time frames. Finite-difference time-domain (FDTD) numerical modelling techniques have recently become commercially available, demonstrating excellent accuracy in predicting the response of complex nano-structures.

Opti-FDTD software, which was described in Chapter 2, was adopted to solve numerically Maxwell's equations and predict the performance of the investigated SWG structures.

Generally, finite-difference time-domain (FDTD) is a common approach to numerically solving partial differential equations [20]. Opti-FDTD is based on the use of central difference approximation in conjunction with the discretization of Maxwell's equations in both the time and space domains. It solves these equations numerically and calculates the electric and magnetic field distributions at each time step using an explicit leapfrog scheme. The FDTD solution is second-order accurate and stable for small time step.

To investigate the effect of the SWG period on light reflection, an SWG structure of constant height equals to 300nm was simulated with the SWG period varied from 50nm to 400nm. The reflection spectrum of the SWG structure was simulated using the FDTD method. Fig. 5.5 shows the simulation steps.

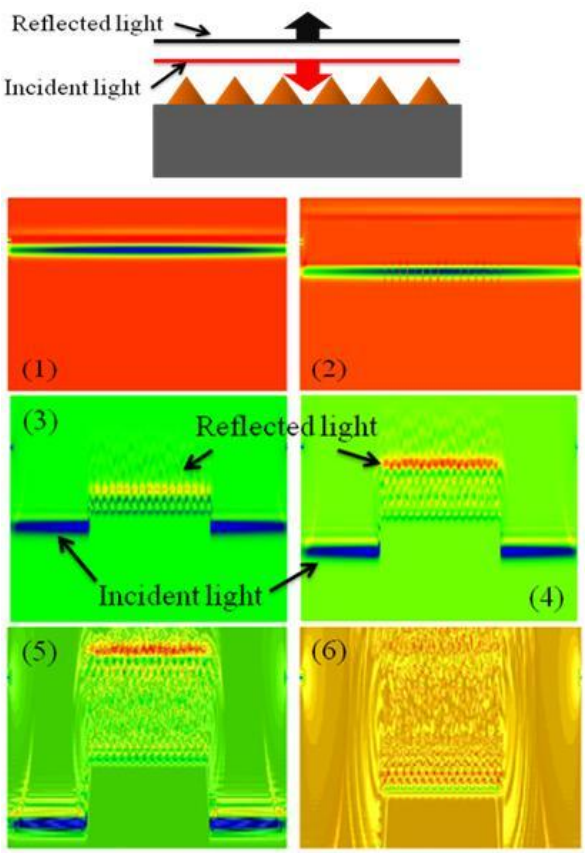

Fig. 5.5 Typical schematic diagram of a conical shaped subwavelength grating (SWG) structure and the simulation outputs obtined through the simulation software for the prediction of the electromagnetic wave propagation across the simulated SWG structure.

Fig. 5.6 shows the effect of grating periods on reflection. For periods of 50nm and 100nm, the corresponding SWG structures result in a reflectance of more than 5%. For a period of 150nm the reflectance is less than 2% up to the 1200nm wavelength and then it increases to 6% for wavelengths up to 1500nm. For a 200nm period, the reflectance is less than 2% for wavelengths below 1300nm wavelength and between 1300nm and 1500nm the reflectance is up to 4%, for a 250nm period it is below 3% over a wide wavelength range. For a 300nm period the reflectance increases to 5% and after 300nm period the reflection for SWG structures with higher periods result in higher reflection. Therefore, the optimum period of the SWG structure is 200 nm.

The reflected light from the SWG structure surface having around 200nm width is reflected at the same angle at which the incoming light strikes the surface. So, most of the light can strike the surface again, rather than being lost and thus reducing the reflection.

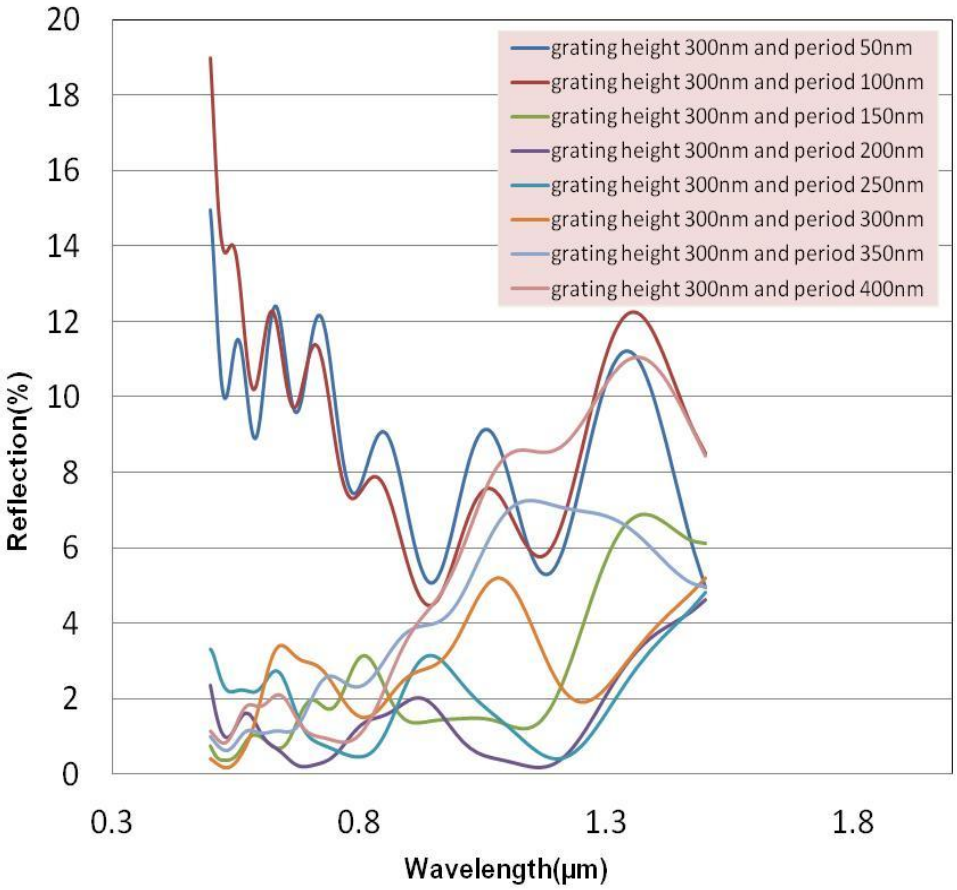

Fig. 5.6 Simulated reflection spectra for SWG structures having a grating height of 300nm and different grating periods.

We then fixed the width and varied the thickness of the gratings and calculated reflection by FDTD method. Fig. 5.7 shows the effect of grating height on reflection. It was found that the taller structure height gives less reflection but is difficult to fabricate and also expensive. At simulations above 300nm grating height we obtained less than 2% light reflection over a wide range of wavelengths.

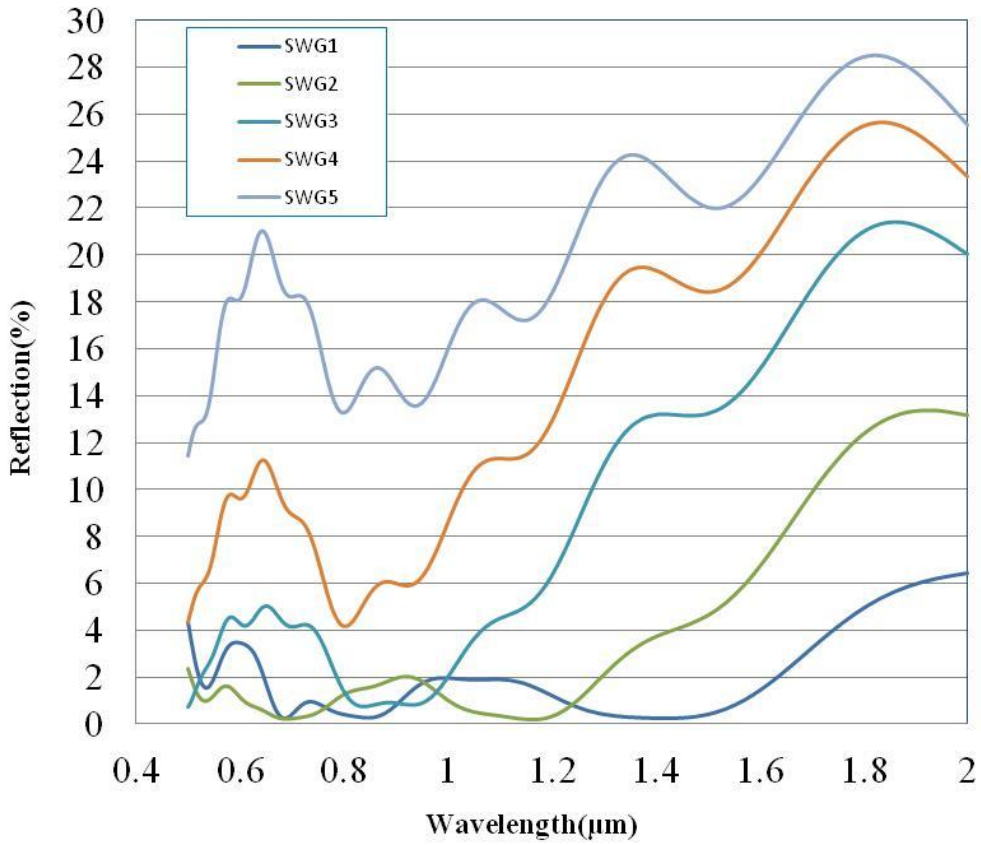

Fig. 5.7 Simulated reflection spectra for SWG structures having a grating period of200nm and different grating heights ofSWG1=400nm; SWG2=300nm; SWG3=200nm; SWG4=150nm and SWG5=100nm.

Longer structure heights can be obtained by controlling etching time. We carried out all our simulations at 300nm grating height and at various grating periods on uniform Ag nanoparticles. Nanoparticles with diameter around 200nm and spacing between nanoparticles as low as possible were our target, as these parameters are suitable for fabrication of SWG structures having same spacing and period of around 200nm, enabling minimum reflection to be attained.

With the obtained experimental data, i.e diameter and spacing between nanoparticles, we simulated(using the Opti-FDTD softeware package developed by Optiwave Inc. [20]) the reflection loss of a predicted SWG structure having a grating

groove width equals to the average nanoparticle diameter and spacing equals to the average spacing between nanoparticles.

Fig. 5.8 shows measured reflectance spectra of fabricated GaN SWGs on GaN/Sapphire corresponding to the etching times of 1, 3, 5, and 9 min. The insets show the SEM images of the fabricated GaN SWSs with different etching times [32]. It is obvious that for a 9-minute etching time the reflectance of the surface is below 5%, in comparison with more than 20% (at around 360nm) for an unpatterned surface.

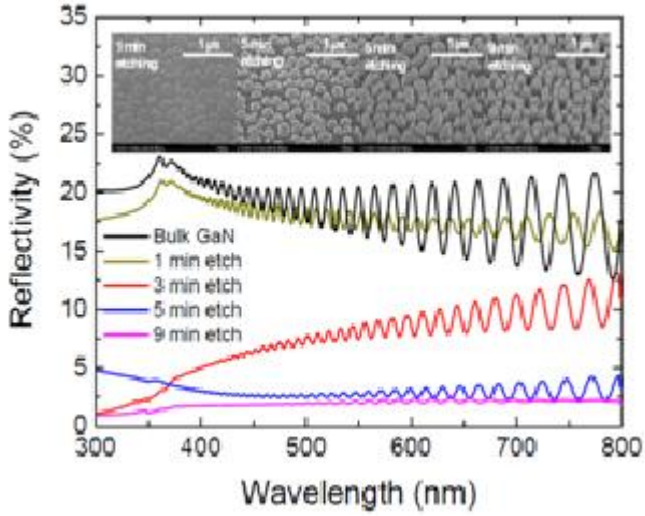

Fig. 5.8 Measured reflectance of the fabricated GaN SWGs on GaN/Sapphire corresponding to the etching times of 1, 3, 5 and 9 min. The insets show the SEM images of the fabricated GaN SWGs with different etching times (Source 32).

The simulated SWG structures that correspond to etching masks experimentally obtained through the annealing of Ag thin films of different thicknesses at different temperatures are plotted in Figs 5.9-11.

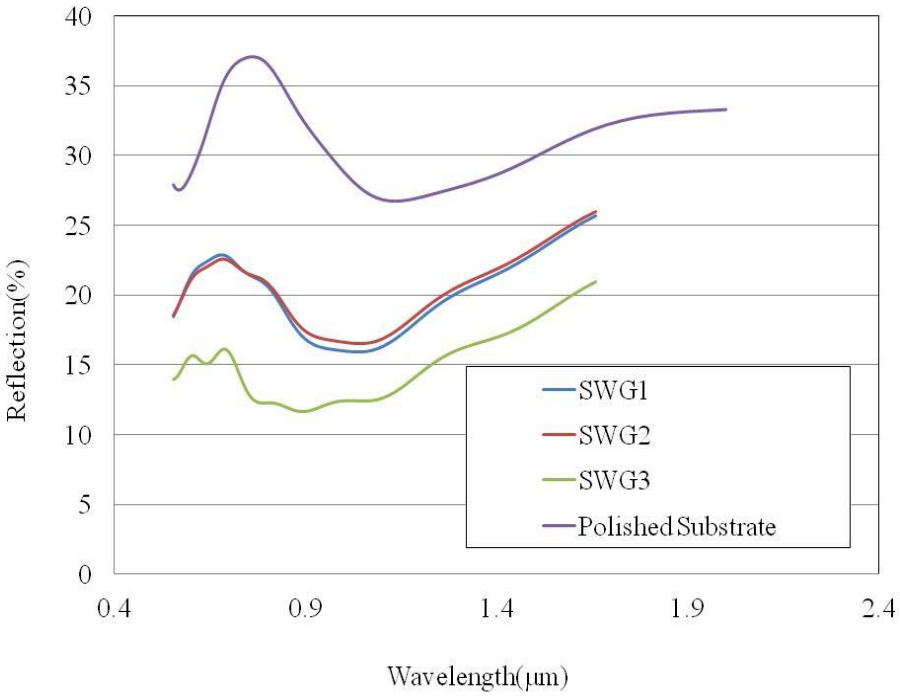

Fig. 5.9 Simulated reflection spectra for GaAs SWG structures obtained with an etching mask realised through the annealing of a 5nm Ag film at different temperatures of SWG1= 623K ; SWG2= 673K and SWG3= 723K. Also shown is the reflection spectrum for a polished unpatterned GaAs substrate.

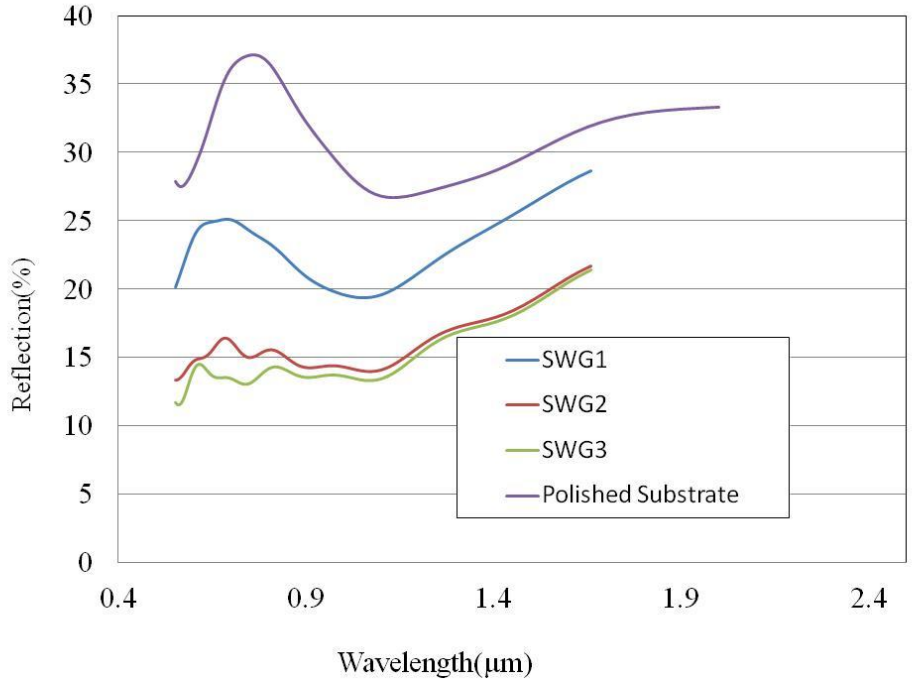

Fig. 5.10 Simulated reflection spectra for GaAs SWG structures obtained with an etching mask realised through the annealing of a 8nm Ag film at different temperatures of SWG1= 523K ; SWG2= 623K andSWG3= 673K. Also shown is the reflection spectrum for a polished unpatterned GaAs substrate.

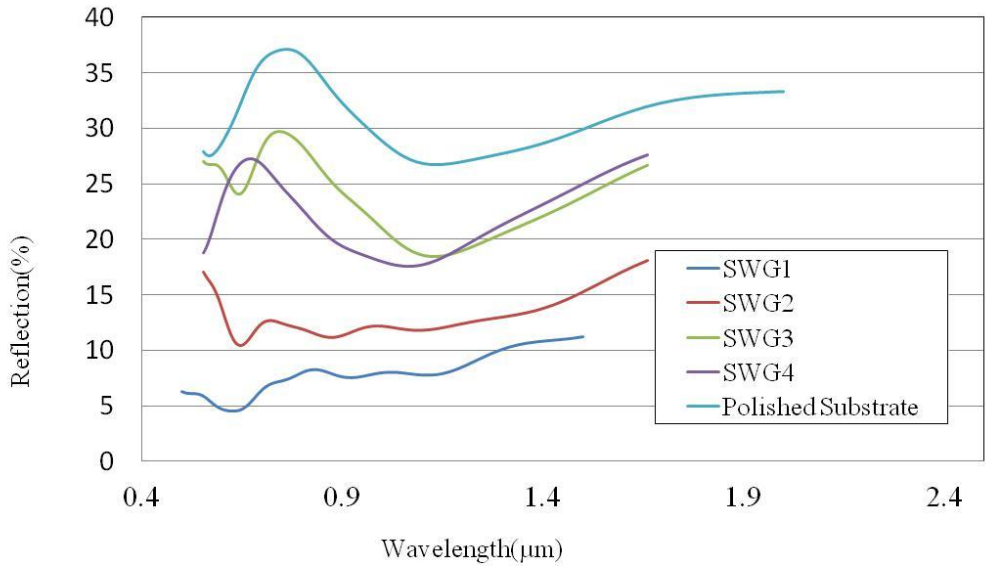

Fig.5.11 Simulated reflection spectra for GaAs SWG structures obtained with an etching mask realised through the annealing of a 10nm Ag film at different temperatures of SWG1= 523K ; SWG2= 573K; SWG3= 623K andSWG4= 673K. Also shown is the reflection spectrum for a polished unpatterned GaAs substrate.

The optimum Ag nanoparticle diameter that minimises the optical reflectance was attained in almost every case through the appropriate annealing temperature. However, the spacing between nanoparticles was higher than the desired value in every situation. Generally, the surface reflectance increases with increasing the average spacing between the nanoparticles, however, a higher spacing affects the grating height(since the etching gas must be applied for a long time to achieve a conical shape). As shown in Fig. 5.9, the average reflectance of a SWG structure developed through an etching mask, obtained by the annealing of a 5nm Ag on a GaAs substrate at 723K, is below 15% over a broadband wavelength span of 400-1300nm, whereas for a polished surface the average reflectance exceeds 27%. Also, the average reflectance of a SWG structure developed through an etching mask, obtained by the annealing of a 8nm Ag on a GaAs substrate at 673K, is below 15% over the 400-1300nm span (Fig. 5.10). On the other hand, the average reflectance of

a SWG structure developed through an etching mask, obtained by annealing of a 10nm Ag on a GaAs substrate at 523K, is below 10% over a wide range of wavelength as shown in Fig. 5.10. The main conclusion obtained from Figs 5.9-11 is that the reflectance of an SWG structure strongly depends on the grating width, grating spacing and grating height. The grating height is typically controlled by adjusting the etching time, while the grating width and spacing can be controlled by optimising the annealing temperature and Ag film thickness. Therefore, by optimising these SWG parameters the reflectance can further be reduced. The other important factor affecting the SWG reflectance is the uniformity of nanoparticle diameter; typically, a nonuniform nanoparticle diameter distribution increases the SWG reflectance.

Fig. 5.12 shows nanoparticle diameter and spacing between nanoparticles for GaAs SWG structures obtained with an etching mask realised through the annealing of a 10nm Ag film at different annealing temperatures. It is found that nanoparticle diameters are almost same after annealing temperature 573K but spacing between nanoparticles increased upto annealing temperature 623K then decreased. Desired diameter is achieved in almost all cases whereas spacings are obtained larger. Minimum reflectance has been found at annealing temperature 523K as the spacing is less and diameter is close to the desired diameter here. The other situation shows higher reflectance in spite of desired diameter as the spacings are larger.

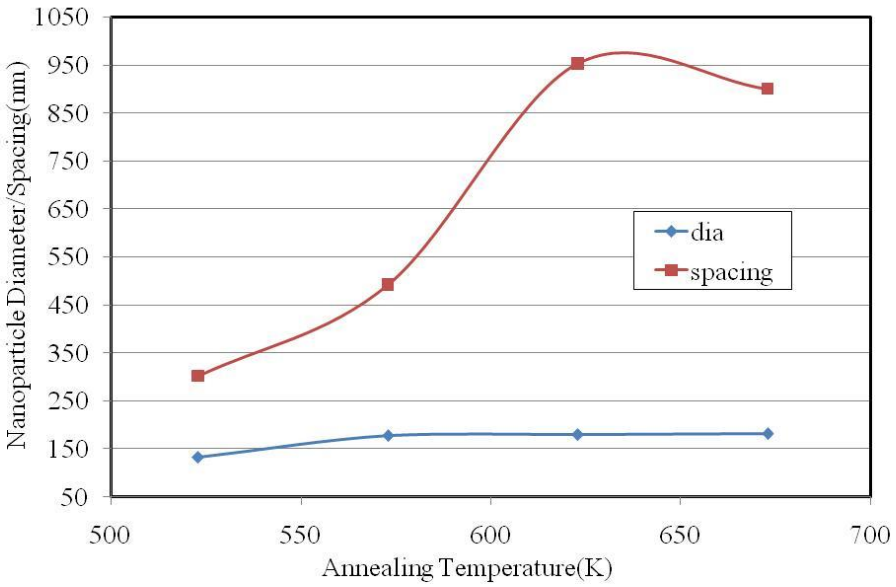

Fig. 5.12 Nanoparticle diameter and spacing for GaAs SWG structures obtained with an etching mask realised through the annealing of a 10nm Ag film at different annealing temperatures.

Fig. 5.13 shows nanoparticle diameter and spacing between nanoparticles for GaAs SWG structures obtained with an etching mask realised through the annealing of a 8nm Ag film at different temperatures. It is found that nanoparticle diameters are close to desired diameter and the variation with annealing temperature is very less whereas the spacings are changes widely and decreased with annealing temperature . Expected reflectance was not obtained here as the spacings are larger in all cases.

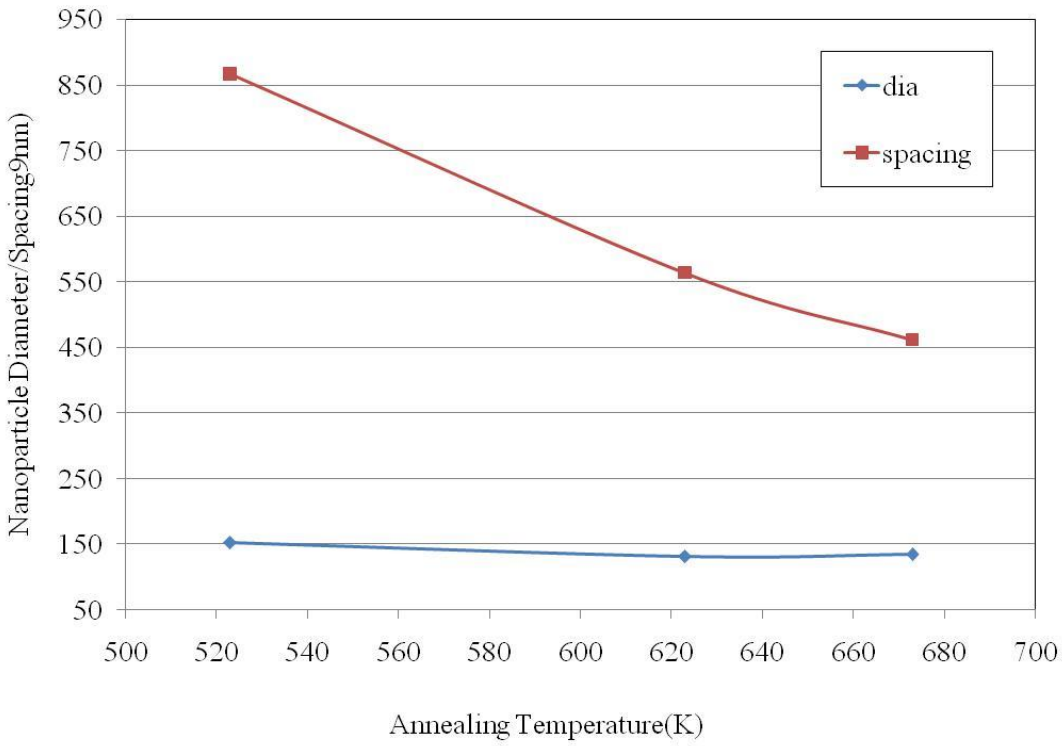

Fig. 5.13 Nanoparticle diameter and spacing for GaAs SWG structures obtained with an etching mask realised through the annealing of a 8nm Ag film at different annealing temperatures.

Fig. 5.14 shows nanoparticle diameter and spacing between nanoparticles for GaAs SWG structures obtained with an etching mask realised through the annealing of a 5nm Ag film at different temperatures. Nanoparticle diameters are found close to desired range and the variation of diameter with annealing temperature is ignorable but the spacings are also larger here and decreased with annealing temperature. Because of larger spacing, expected reflectance was not obtained here.

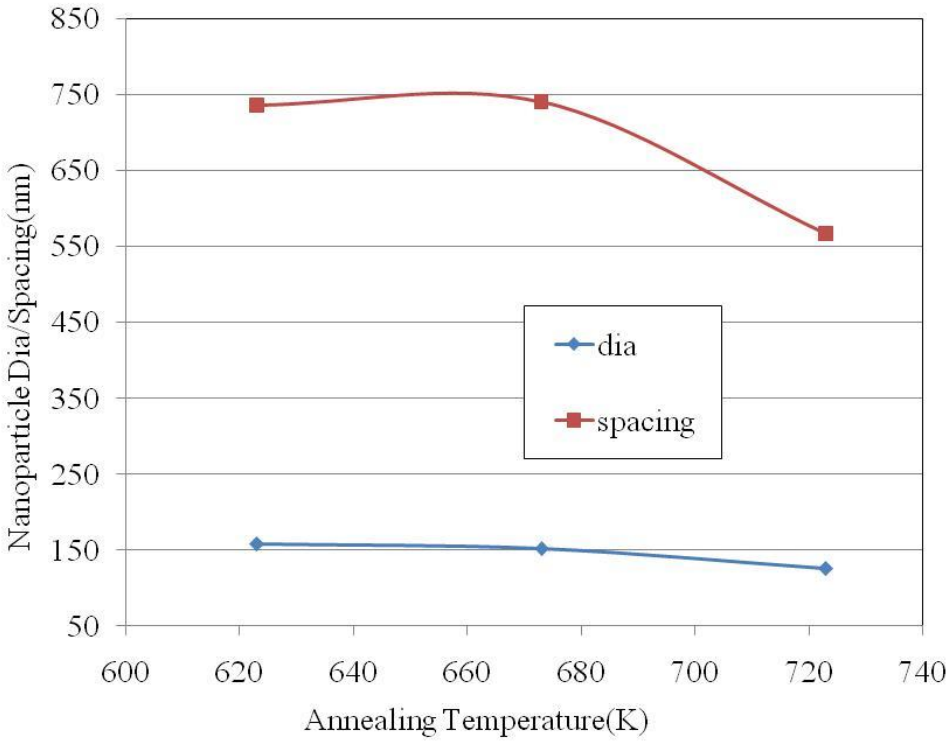

Fig. 5.14 Nanoparticle diameter and spacing for GaAs SWG structures obtained with an etching mask realised through the annealing of a 5nm Ag film at different annealing temperatures.

We have also observed the dependency of nanoparticle diameter and spacing on Ag film thickness. Fig. 5.15 shows nanoparticle diameter for GaAs SWG structures obtained with an etching mask realised through the annealing of different thicknesses samples. It is observed that diameter varies from 130nm to 185nm which is good for minimal reflectance.

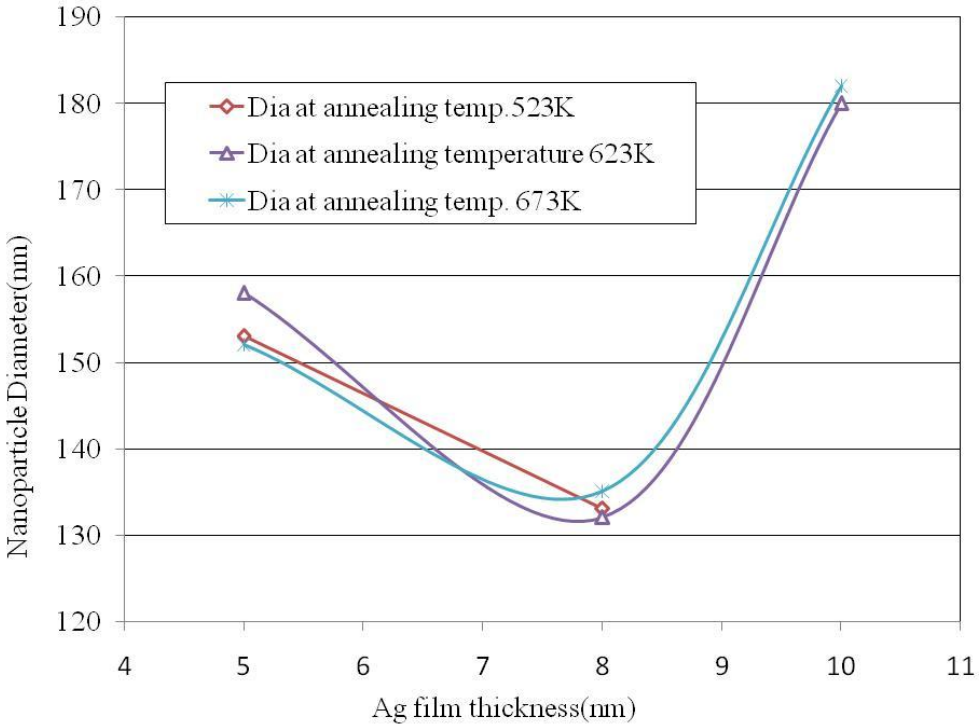

Fig.5.15 Nanoparticle diameter for GaAs SWG structures obtained with an etching mask realised through the annealing of different thicknesses Ag film at different annealing temperatures.

Figure 5.16 shows nanoparticle spacing for GaAs SWG structures obtained with an etching mask realised through the annealing of different thicknesses samples. Less spacing obtained through the annealing of a 8nm Ag on GaAs substrate at annealing temperature 623K and 673K.

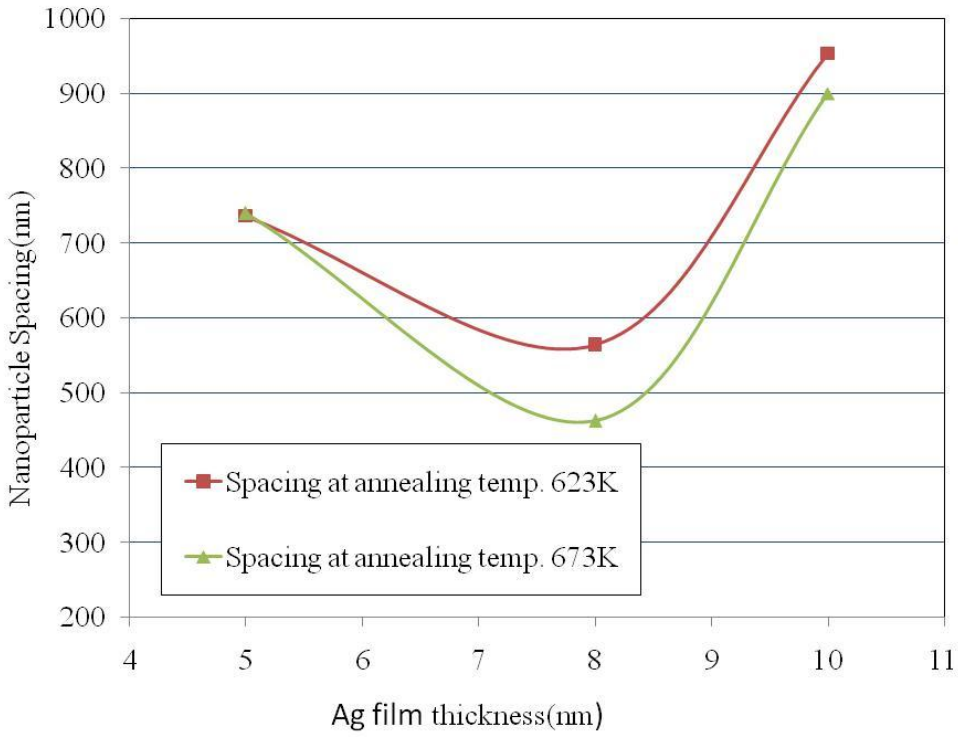

Fig 5.16 Nanoparticle spacing for GaAs SWG structures obtained with an etching mask realised through the annealing of different thicknesses Ag film at different annealing temperatures.

Our results show that nanoparticle diameter varies from 100-200nm, however the spacing between nanoparticles varies upto 950nm. Obtained diameter range is very good for less reflectance but spacings between nanoparticles are large that give higher reflectance. Reflectance can be reduced further by reducing spacing between nanoparticles.

5.2.5 Conclusion:-

Ag thin films with different thicknesses have been deposited on semiconductor substrates and annealed at different temperatures to fabricate Ag nanoparticles that can be used to develop cost-effective AR coatings for semiconductor devices. We have found that the desired diameter and spacing between nanoparticles can be

achieved by controlling the annealing temperature and Ag film thickness and that the coated substrates can ultimately be used to fabricate SWG structures with the desired grating width and spacing between gratings thereby ensuring minimum reflection. The desired nanoparticle diameter is obtained in almost all cases but the spacing varies widely. Therefore, by reducing the space between nanoparticles we can reduce the reflection even more.

5.3 Silver (Ag) nanoparticle arrays on Silicon (Si) substrates:-

To fabricate silver naoparticles, Ag thin films of different thicknesses 10nm, 8nm and 5nm are deposited on Si substrates using RF magentron sputtering system and then the deposited samples are annealed in an oven at 523K, 573K, 623K, 673K and 723K for 30 minutes. SEM images of the annealed samples areobtained and characterized by ImageJ software. The annealed samples with their calculated parametersarethen used to design SWG structureswhich can be developed through etching process. The reflection loss of the SWG structures are simulated by FDTD simulation method and compared with flat substrates.

5.3.1 Formation of particle arrays:-

There are two steps of the formation of particle arrays (i) Thin film deposition on Silicon(Si) substrates using the sputtering method and (ii) Annealing of the thin film on Silicon(Si) substrates.

(i) *Thin film deposition on Silicon(Si) substrates by sputtering method*: Deposition of Ag metal film upon silicon(Si) substrates were performed using the RF magnetron sputtering system described in chapter 3. The RF magnetron sputtering system is a widely used method, and is based on a physical vapour deposition process that can fabricate high quality films at low operating pressure. Substrates and target material are placed inside the system as shown in figure 3.1, both work as anode and cathode respectively. An electric field accelerated the electrons between the substrate and the target where Argon (Ar) atoms are ionised to Ar^+ which sputter target atoms. Target atoms transversed the vacuum chamber and condensed on the substrates producing the desired thin film result. 10nm, 8nm and 5nm Ag thin films on Si were fabricated by using the RF

sputtering system. Film thicknesses were monitored during the sputtering process with the in-situ laser reflectometry system. During the thin film deposition s-polarized light is used to impinge on the middle of substrate and the thickness of the growing film is measured by capturing the reflected power by the detector using "Real-Time Thickness Control for Multilayers" software made at ECU [23]. The conditions of the RF magnetron sputtering system at which Ag film is deposited on silicon(Si) substrates are listed in Table 5.3.

Table 5.3

Operational conditions of RF Magnetron Sputtering system for Silver (Ag) deposition on Si substrate

Target	Ag
Substrate	Silicon(Si)
Sputtering Gas & Pressure	Argon (Ar), 1-2mTorr
R.F Power Density	0.98-1.41
Base Pressure	2-3E^{-06}Torr (High Vacuum)
Substrate surface temperature during deposition process	Room temperature (below 30°C)
Substrate Stage Rotation	32-36rpm
Substrate Target distance	18-20cm

ii) Annealing of thin film on Silicon (Si) substrate: The Ag films were then annealed by heating it first then cooling it. As described in Chapter 3, heat provides energy for the materials to break the bonds of atoms and increases the rate of diffusion of the material's atoms during annealing. The diffusion of the material progresses towards its equilibrium state thus redistributing and destroying the dislocations of the Ag atom sand increasing their ductility. Also, the annealing process reduces the Gibbs-free energy needed for initiating the Ag nanoparticle formation. This reduction is called "stress

relief", which is a spontaneous process at high temperature, but very slow at room temperature [24, 25].

A conventional temperature ramp-controlled box furnace oven was used in our experiment to fabricate Ag nanoparticles through three steps annealing process which was described in section 3.2

The annealing process was performed at different temperatures 523K, 573K, 623K, 673K and 723K for a constant time of 30 minutes and the size and distance between the nearest nanoparticles were observed. The aim of this project was to discover (i) the metal film thickness and annealing temperature at which nanoparticles with diameter range around200nm and spacing between the nearest metal nanoprticles as low as possible can be formed, and (ii) realisation of SWG structures with a grating width and grating distance in the same range of nanoparticle diameter and spacing between nanoparticles that satisfies the condition of less reflection loss.

5.3.2 Characterization of particles and their arrays:-

The images of the annealed samples were taken using Scanning Electron Microscopy (SEM) to observe particle size and characterisation. This is a time consuming and expensive method, but sample preparation is relatively easy and it is possible to measure up to 1nm particle. The sample must be placed under the vacuum and should be electrically conductive. For this technique, a high energy electron beam is used and the beam is scattered over the surface. Then the back scattering of the electrons is observed.

Several samples were placed in the vacuum chamber at the same time and the sample images were observed. Fig. 5.17, 5.18 and 5.19 shows the SEM images recorded in this experiment:

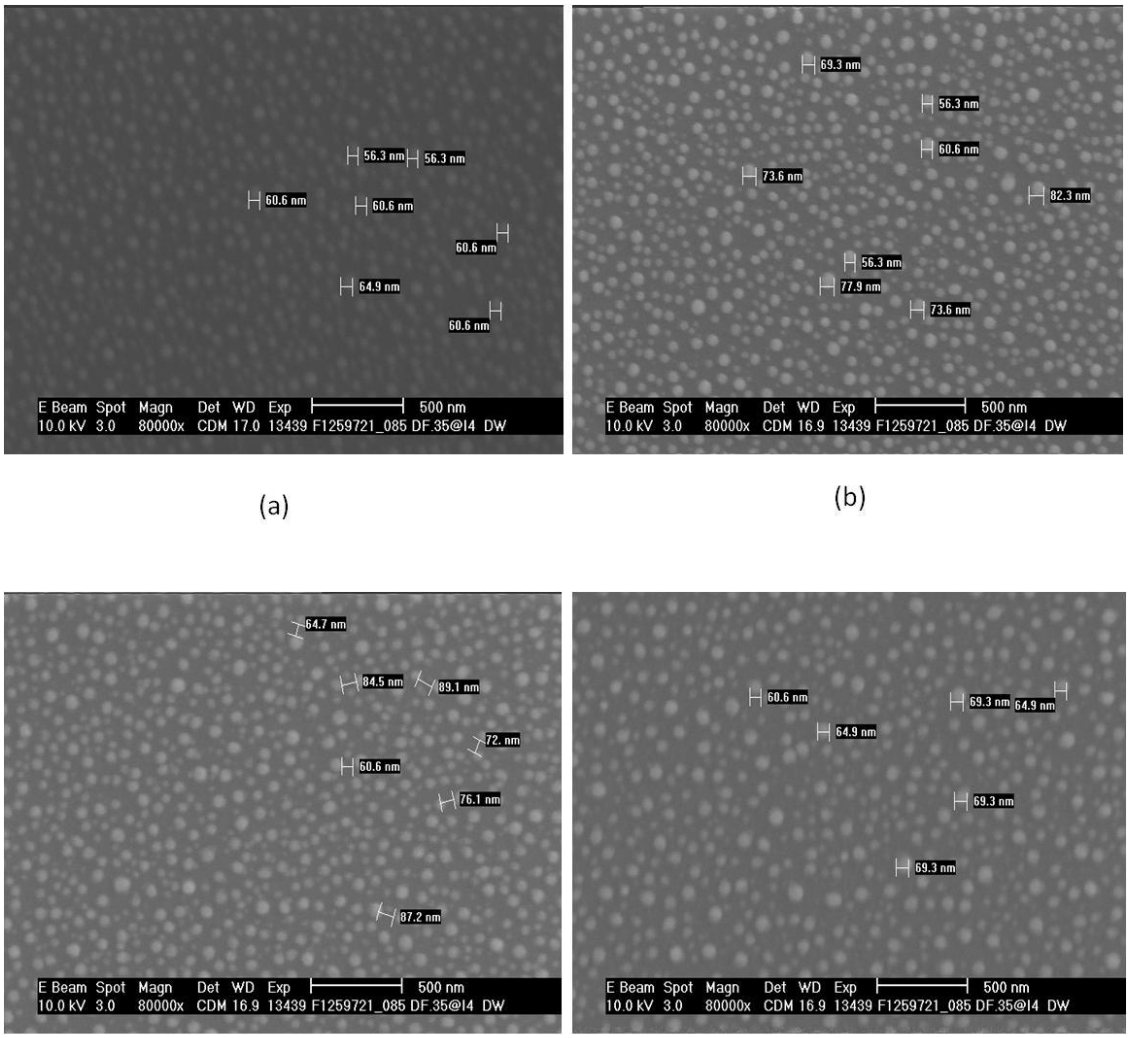

Fig. 5.17 SEM image of Ag nanoparticles obtained by depositing an 5nm Ag thin film on a Si substrate and annealing at (a) 523K, (b) 573K, (c) 623K and (d) 673K.

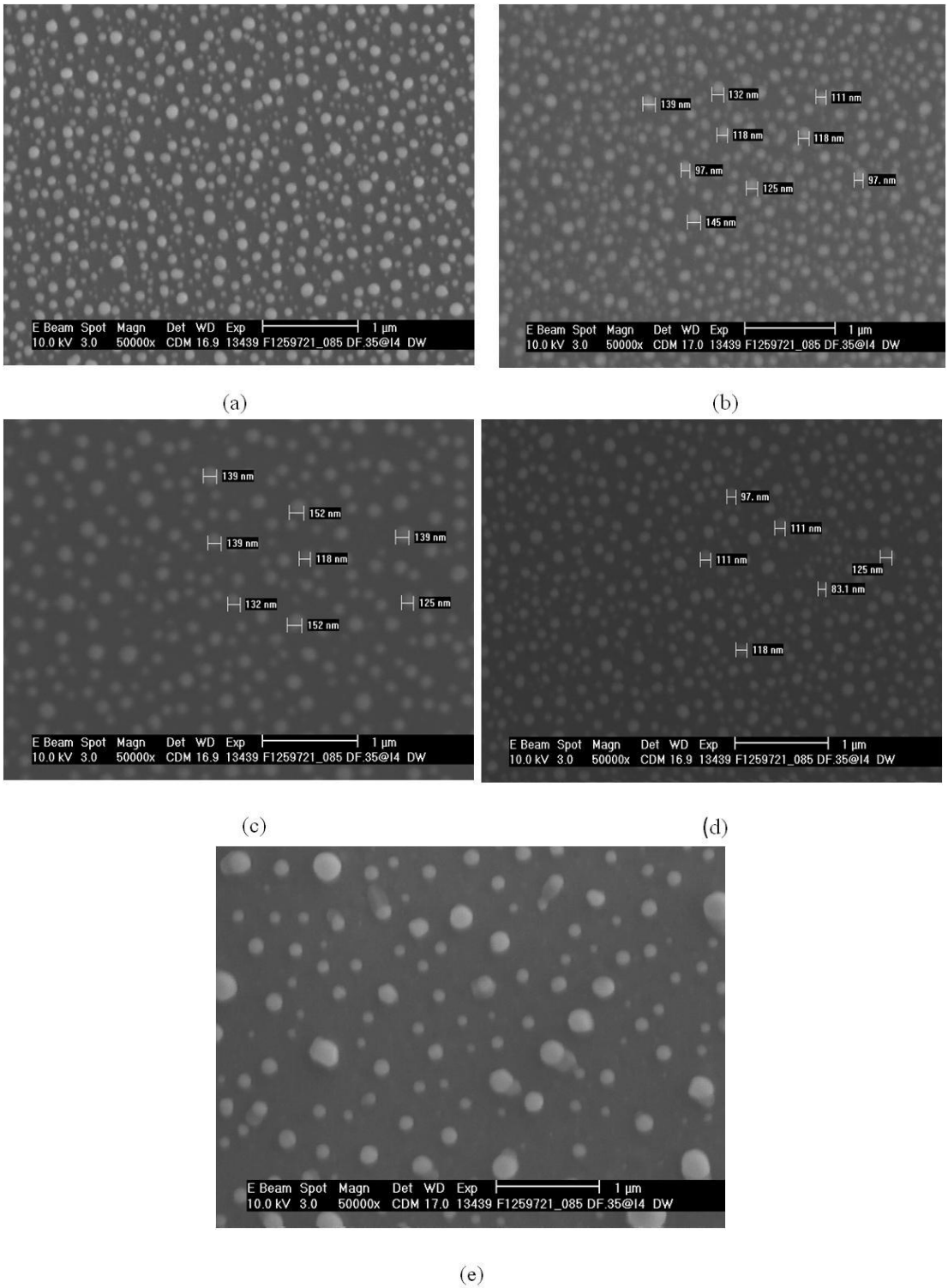

Fig. 5.18 SEM image of Ag nanoparticles obtained by depositing an 8nm Ag thin film on a Si substrate and annealing at (a) 523K, (b) 573K, (c) 623K, (d) 673K and (e) 723K.

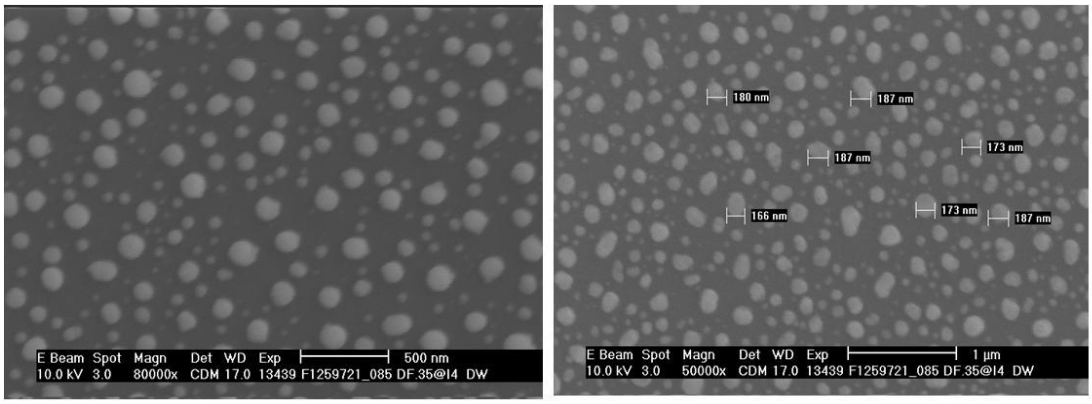

(a) (b)

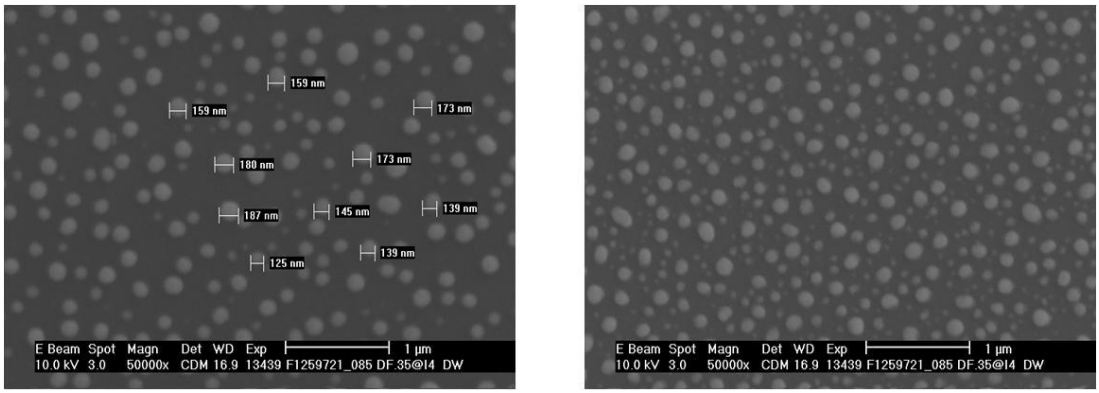

(c) (d)

Fig. 5.19 SEM image of Ag nanoparticles obtained by depositing an 10nm Ag thin film on a Si substrate and annealing at (a) 523K, (b) 573K, (c) 623K and (d) 673K.

5.3.3 Experimental characterization results:-

Nanoparticle diameter and spacing between nanoparticles are calculated by using ImageJ software described in section 5.2.2 and are listed in Table 5.4.

Table : 5.4

Different parameters of Ag nanoparticles on Silicon (Si) substrates

Thickness of Ag film on Si substrate (nm)	Annealing Temp.(K)	Weighted Average Diameter of nanoparticles (nm)	No. of nanonoparticles	Space between Nanoparticles (nm)
10	523	118	166	217
	573	136	147	246
	623	160	91	492
	673	114	160	216
8	523	85.4	206	406
	573	100.6	155	240
	623	146.9	112	328.8
	673	93.4	196	187
	723	145	69	488
5	573	37.7	390	75
	623	37.2	394	77
	673	54.4	248	114
	723	54.14	290	101

From Table 5.4 it is seen that for 10nm Ag on Si substrate, the weighted average diameters are 118nm, 136nm, 160nm, 114nm and average spacing between nanoparticles are 217nm, 246nm, 492nm, 216nm at annealing temperatures 523K, 573K, 623K and 673K respectively, for 8nm Ag on Si substrate, the weighted average diameters are 85.4nm, 100.6nm, 146.9nm, 93.4nm, 145nm and the average spacing between nanoparticles are 406nm, 240nm, 328.8nm, 187nm, 488nm at annealing temperatures 523K, 573K, 623K, 673K and 723K, respectively, and for 5nm Ag on Si substrate the weighted average diameters are 37.7nm, 37.2nm, 54.4nm, 54.14nm and the average spacing between nanoparticles are 75nm, 77nm, 114nm, 101nm at annealing temperatures 573K, 623K,673K and 723K, respectively.

5.3.4 SWG Simulation:-

Ag nanoparticles on Si substrates were formed for the fabrication of SWG structures. A period around 200nm for Ag on GaAs substrate gives minimum reflectance that stated in section 5.2.4. We obtained the same result through the simulation of Si SWG structure using Opti-FDTD method which was carried at a constant grating height 300nm. Fig. 5.20 shows the simulated reflection spectrum of the SWG structure, confirming that for a period of around 200nm the reflectance is less than 2% over a wide range of wavelengths. Note that Ag nanoparticles on Silicon(Si) substrates with a spacing as low as possible and an average nanoparticple diameter around 200nm were our target, as these parameters are suitable for fabrication of a SWG structures having same spacing and a grating width the same as the nanoparticle diameter, enabling minimum reflection loss to be attained.

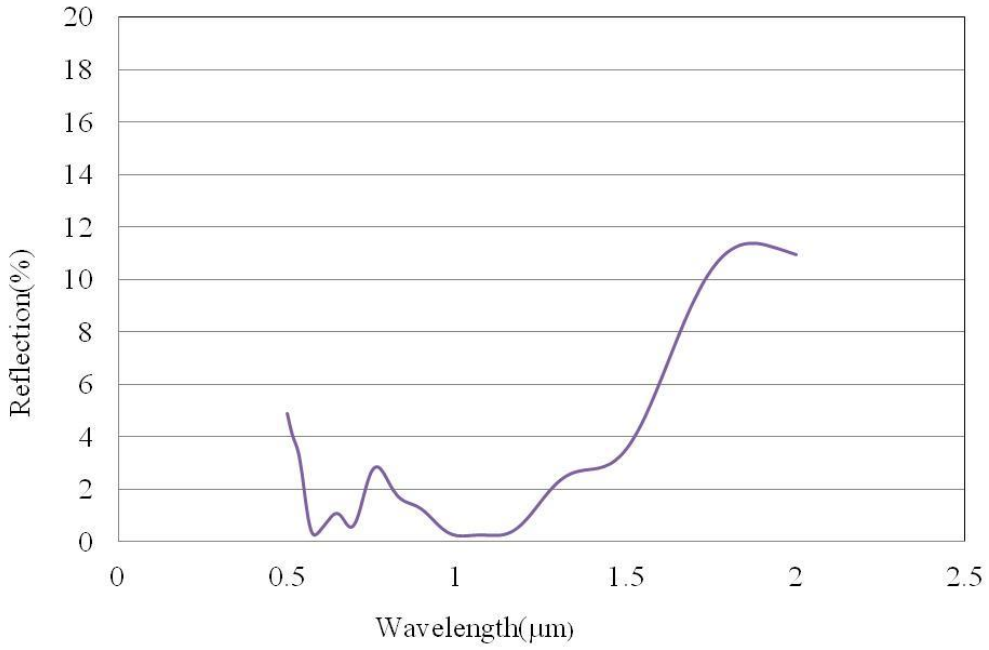

Fig. 5.20 Simulated reflection spectrum for a Si SWG structure having a period of 200nm and grating height of 300 nm.

We then varied the thickness of the gratings but maintained a constant period, and the reflection spectrum was calculated using the same FDTD method. Fig. 5.21 shows the effect of grating heights on reflection. We also found that the taller grating height results in less reflection. For grating heights above 300nm less than 5% reflection is attained over a wide range of wavelengths, and hence, we fixed the grating height at300nm for all subsequent simulations.

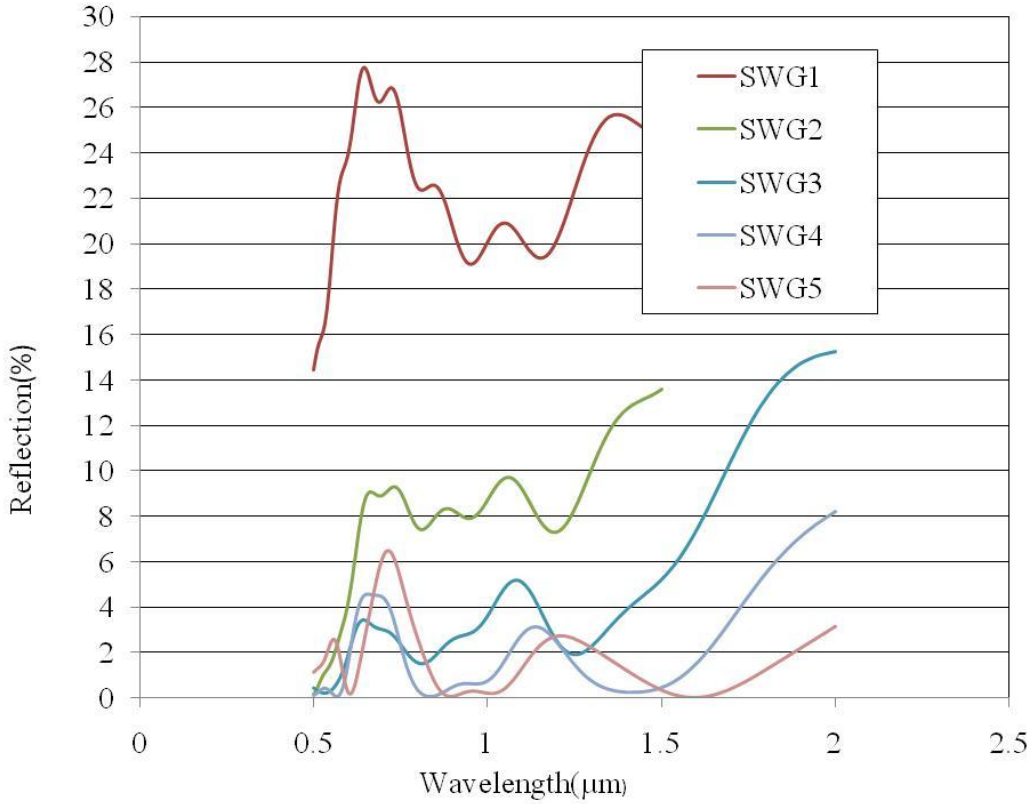

Fig. 5.21 Simulated reflection spectra for SWG structures having a grating period of 200nm and different grating heights of SWG1=100nm; SWG2=200nm; SWG3=300nm; SWG4=400nm and SWG5=500nm.

With the obtained experimental data, i.e average diameter and spacing between nanoparticles, we simulated(using the Opti-FDTD softeware package developed by Optiwave Inc. [20]) the reflection of a predicted SWG structure having a grating groove width equals to the average nanoparticle diameter and spacing equals to the

average spacing between nanoparticles. The steps for simulatingthe propagation of the electromagnetic waves across the sample areshown in Fig.5.5.We carried out all our simulations based on uniform Ag nanoparticles, at 300 nm grating height and at various grtaing periods.

The simulated SWG structures that correspond to etching masks experimentally obtained through the annealing of Ag thin films of different thicknesses at different temperatures are plotted in Figs 5.22-5.24.

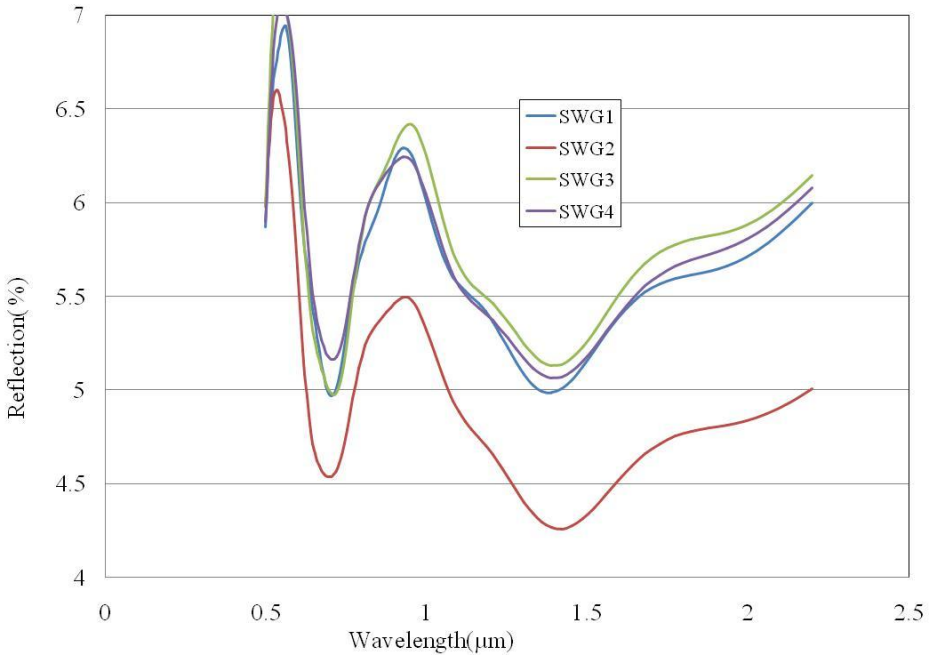

Fig. 5.22 Simulated reflection spectra for Si SWG structures obtained with an etching mask realised through the annealing of a 5nm Ag film at different temperatures of SWG1= 573K ; SWG2= 623K ; SWG3= 673K and SWG4= 723K.

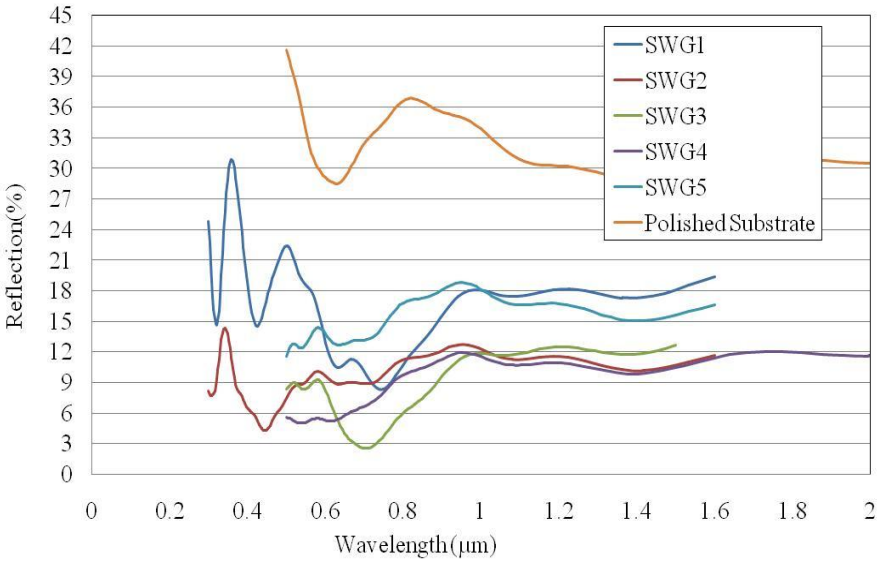

Fig. 5.23 Simulated reflection spectra for Si SWG structures obtained with an etching mask realised through the annealing of a 8nm Ag film at different temperatures of SWG1= 723K ; SWG2= 673K ; SWG3= 623K; SWG4= 573K and SWG5=523K, as well as reflection spectrum for a polished unpatterned Si substrate .

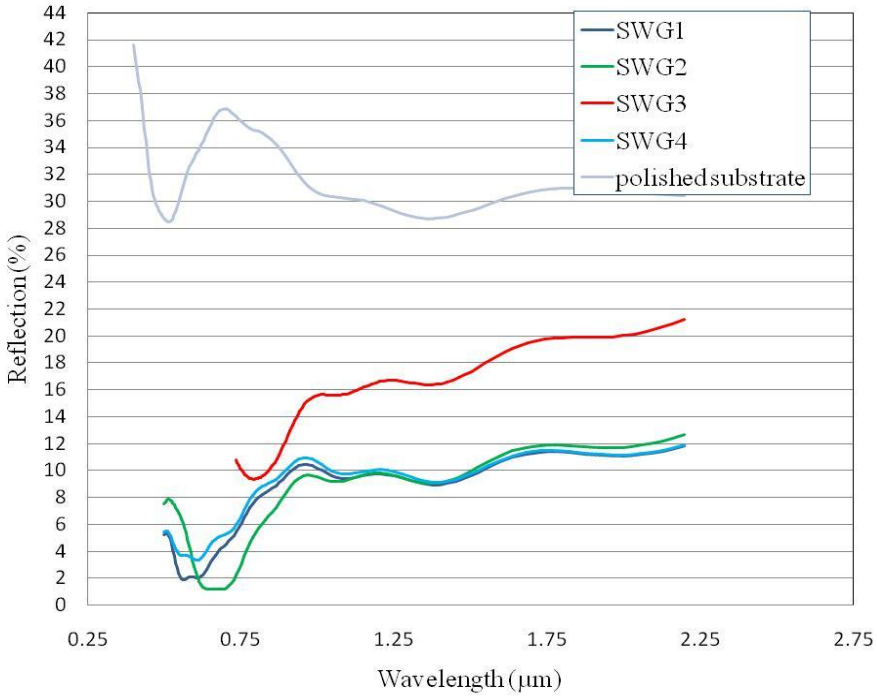

Fig. 5.24 Simulated reflection spectra for Si SWG structures obtained with an etching mask realised through the annealing of a 10nm Ag film at different temperatures of SWG1= 523K ; SWG2= 573K ; SWG3= 623K and SWG4= 673K. Also shown is the reflection spectrum for a polished unpatterned Si substrate.

Fig. 5.24 indicates that the average reflectance of a SWG structure developed through an etching mask, obtained by annealing a 10nm Ag film on a Si substrate at 523K is2-12%,at 573K the reflectance is 1-10% over a wide range of wavelength and at 673K the reflectance is 3-12%. Also, the reflectance of a SWG developed through an etching mask, obtained by annealing 8nm Ag film on a Si substrate at 623K is 3-10% over a wide range of wavelength, at 573K the average reflectance is below12% and at 673K it is below12% as well (Fig. 5.23).On the other hand the reflectances of a SWG structure developed through an etching mask, obtained by annealing a 5nm Ag film on a Si substrate annealed at 573K, 623K, 673K and 723K are 4-7% (Fig. 5.22),whereas the reflectance of a polished surface exceeds 28%.

The dependency of both the nanoparticle diameter and spacing on the annealing temperature and Ag film thickness was also investigated here.

Fig. 5.25 shows the nanoparticle diameter and spacing between nanoparticles for a Si SWG structures obtained with an etching mask realised through the annealing of a 10nm Ag film at different temperatures. It is obvious that the nanoparticle diameter that can be attained varies from 114nm to 160nm, and the spacing between nanoparticles increases, reaching a maximum level at the annealing temperature 623K before decreasing. It is important to note that while the obtained average diameters are close to the desired average diameter the average spacing between the nanoparticles are larger than the desired one. The average reflectances obtained at the annealing temperatures 523K, 573K and 673K are lower than the average reflectance obtained at the annealing temperature 623K. This is because the spacing

is higher at the annealing temperature 623K [Fig.5.24].

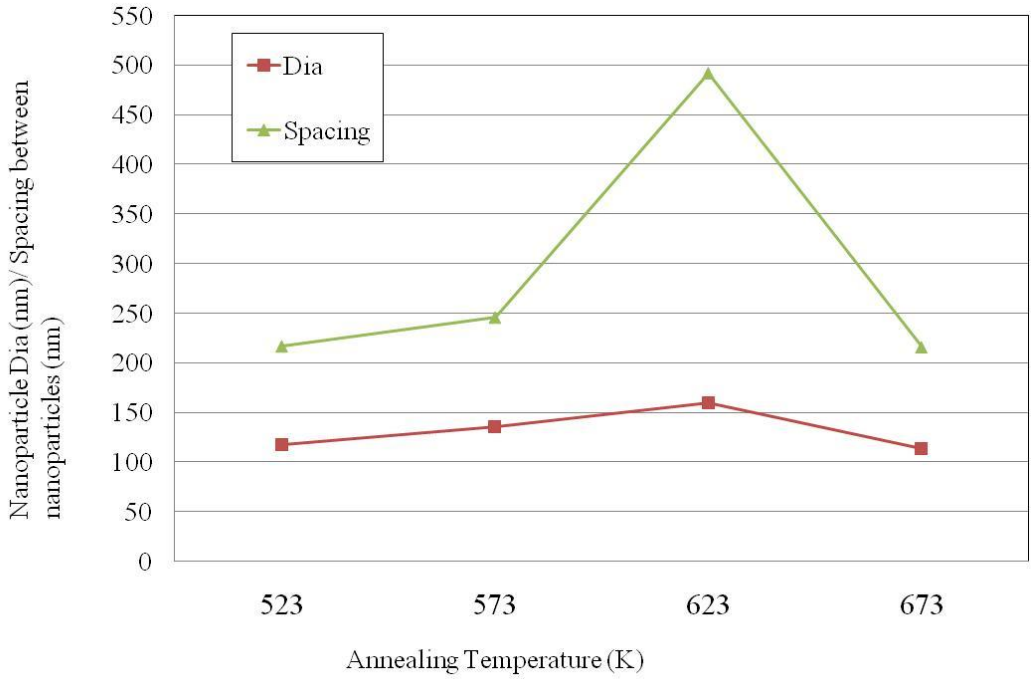

Fig 5.25 Nanoparticle diameter and spacing for Si SWG structures obtained with an etching mask realised through the annealing of a 10nm Ag film at different annealing temperatures.

Fig. 5.26 shows the nanoparticle diameter and spacing between nanoparticles for Si SWG structures obtained with an etching mask realised through the annealing of a 8nm Ag film at different temperatures. It is found that nanoparticle diameters varied from 85nm to 147nm only, but the spacing between the nanoparticles increased upto around 488nm. Also noted in Fig. 5.25 that the spacings between nanoparticles are comparatively lower at the annealing temperatures 573K and 673K.The average reflectance obtained at the annealing temperatures 573K and 673K are also less compared to other annealing temperatures [Fig.5.23].

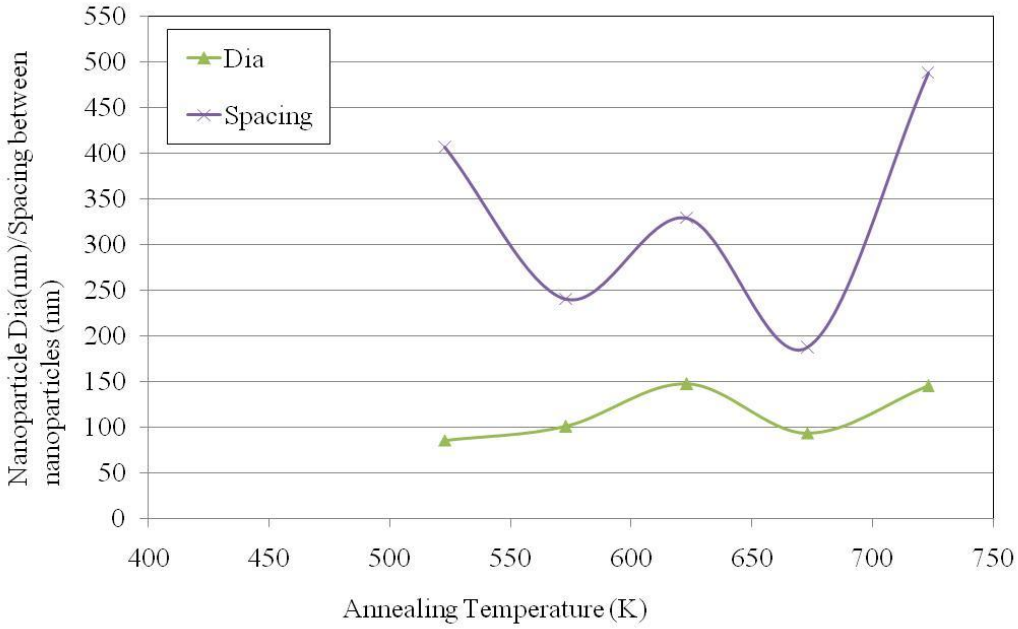

Fig 5.26 Nanoparticle diameter and spacing for Si SWG structures obtained with an etching mask realised through the annealing of a 8nm Ag film at different annealing temperatures.

Fig. 5.27 shows the nanoparticle diameter and spacing between nanoparticles for Si SWG structures obtained with an etching mask realised through the annealing of a 5nm Ag film at different temperatures. It is found that average nanoparticle diameter is around 50nm and a spacing range below 120nmis obtained for all annealing temperatures.4-7% reflectance is achieved for all annealing temperatures (Fig. 5.22). This is mainly becausethe spacings between nanoparticles are very low.

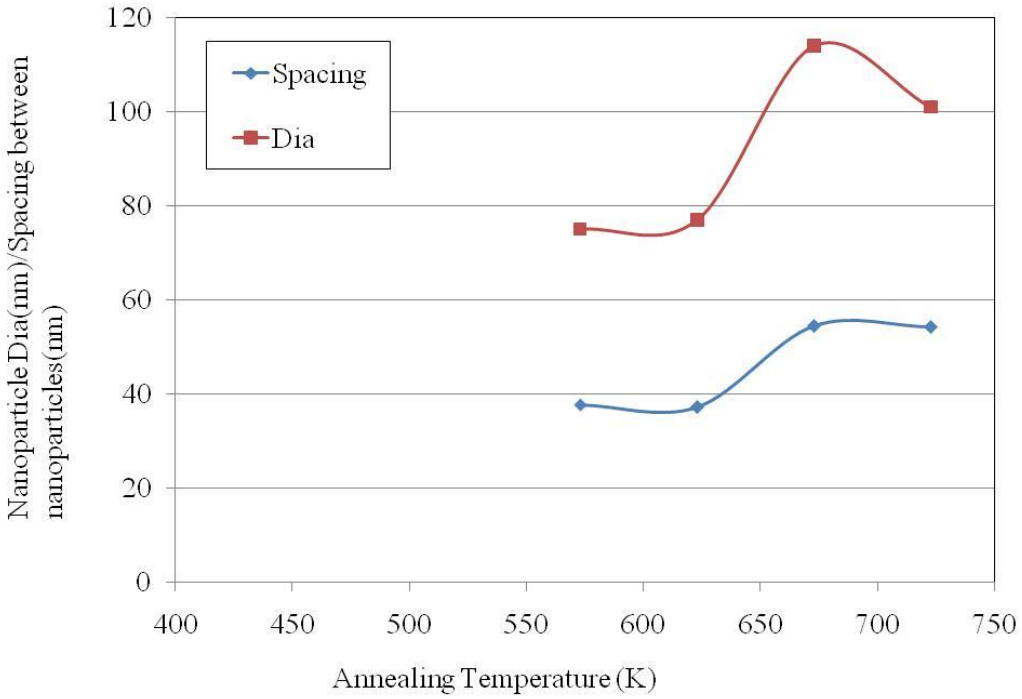

Fig. 5.27 Nanoparticle diameter and spacing for Si SWG structures obtained with an etching mask realised through the annealing of a 5nm Ag film at different annealing temperatures.

We also investigated the dependency of the nanoparticle diameter and spacing on the Ag film thickness. Fig. 5.28 shows the nanoparticle diameter for Si SWG structures obtained with an etching mask realised through the annealing of Ag films of different thicknesses. It is observed that typically the average diameter increases with increasing the film thickness.

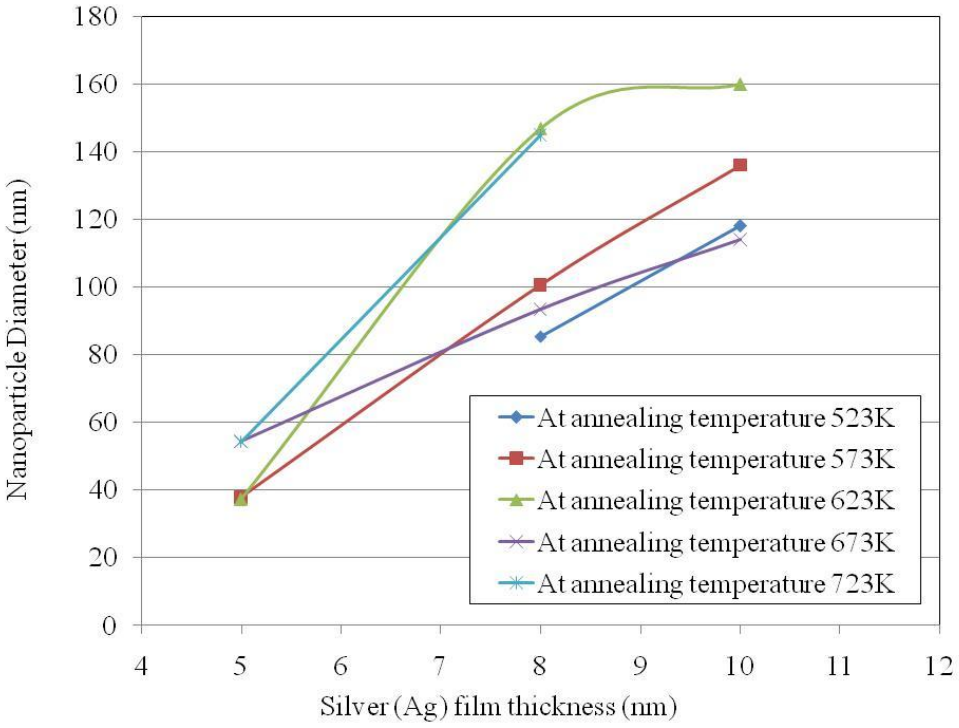

Fig. 5.28 Diameter of Ag nanoparticles on Si SWG structures obtained with an etching mask realised through the annealing of different thicknesses Ag film on Si substrates at different annealing temperatures.

Based on the experimental results shown in Fig. 5.28,we recommend the use of a higher Ag film thickness to attain the target diameter of around 200nm. Fig. 5.29 shows the spacing between the nanoparticle versus the Ag thin film thickness for different annealing temperatures. It is obvious that the spacing also increases with increasing the Ag film thickness. Therefore, to reduce the spacing, it is recommended that the Ag film thickness should be reduced. It is obvious from Figs 5.28 and 5.29 that in order to fabricate low reflection SWG structures it is important to control the spacing between the nanoparticles to the lowest possible and use an Ag film of thickness exceeding 13nm annealed at around 573K.

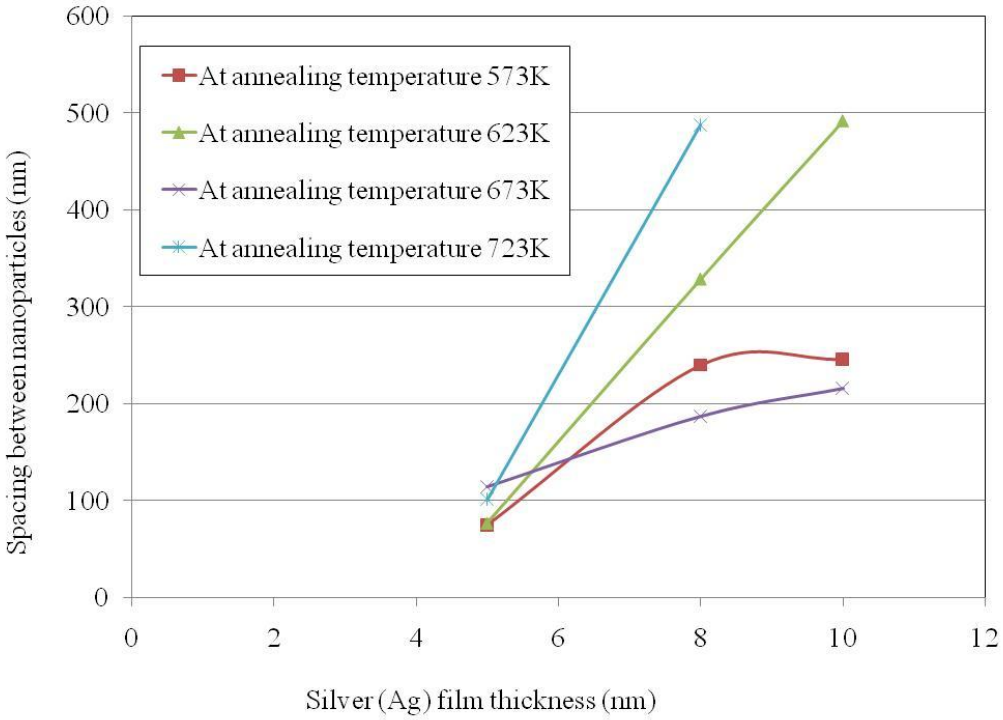

Fig. 5.29 Spacing between Ag nanoparticles on Si SWG structures obtained with an etching mask realised through the annealing of different thicknesses Ag film on Si substrates at different annealing temperatures

5.3.5 Conclusion:-

Ag thin films of various thicknesses have been deposited on semiconductor substrates and annealed at different temperatures to fabricate Ag nanoparticles that can be used to develop cost-effective AR coatings for semiconductor devices. We found that the desired diameter and spacing between nanoparticles can be achieved by controlling annealing temperature and Ag film thickness and that the coated substrates can ultimately be used to fabricate low-reflectance SWG structures having the desired grating width and spacing. To achieve SWG with reflectance as low as 1%, it is recommended to use an Ag film thickness, of around 13nm annealed at a temperature of around 573K. SWG structures have application in high-efficiency solar cells.

Chapter 6

Conclusion

We have investigated the design and development of Ag nanoparticles that can be used as etch masks for the development of antireflection subwavelength grating (SWG) structures. The silver thin film thickness and the annealing temperature have been optimised in order to attain the appropriate Ag nanoparticle diameter and spacing distributions that minimise the reflectance of the SWG structures. Based on the use of different Ag film thicknesses deposited on Silicon (Si) and Gallium Arsenide (GaAs) semiconductor substrates and annealed at different temperatures, we have predicted, using a Finite-Difference Time Domain (FDTD) software package, the performance of different subwavelength grating structures that can be developed using dry and isotropic etching of semiconductor substrates.

Both the optimum Ag nanoparticle diameter and spacing have been found to around 200nm while the optimum height of the nanoparticles has been found to be around 300nm. Such optimum parameters enable SWG structures of reflectance as low as 5% over a broad solar spectrum range to be achieved.

The simulation and experimental results presented in this thesis will benefit applications requiring cost-effective development of antireflective SWG structures.

References

[1] J. H. Schmid, P. Cheben, S. Janz, J. Lapointe, E. Post, A. Delage, A. Densmore, B. Lamontagne, P. Waldron and D.-X. Xu, "Subwavelength grating structures in planar waveguide facets for modified reflectivity", proc. of SPIE Vol 6796 67963E-1, The International Society for Optics and Phonotics, USA, 2007.

[2] H. Kikuta, H. Toyota and Wanji Yu, "Optical elements with subwavelength structured surfaces", Optical Review Vol 10 (2), pp. 63-73, The Optical Society of Japan, 2003.

[3] Y. M. Songand, Y. T. Lee, "Simulation of antireflective subwavelength grating structure for optical device applications", Proceedings of the 9th International Conference on Numerical Simulations of Optoelectronic Devices (NUSOD'09), pp. 103-104,Gwangju Institute of Science and Technology, Republic of Korea,2009.

[4] Y. M. Song, S. J. Jang, J. S. Yu, and Y. T. Lee, "Bioinspired parabola subwavelength structures for improved broadband antireflection," Small (Journal), vol. 6, pp. 984-987, Wiley-VCH, Germany, 2010.

[5] G. Knier, "How does Photovoltaics Work?", Science News, NASA Science, (Sighted on May 2010).

[6] J. Mathew, Parry-Hill, T. Robert, Sutter and Michael W. Davidson, "Physics of Light and Color", Interactive Java Tutorials, Molecular Expressions™ Microscopy Primer", (Sighted on 27/05/2010).

[7] Energy Information Centre, "Photovoltaic Cells", Energy Victoria.

[8] H. A. Macleod, "Thin-film optical filters", *2nd ed*, Adam Hilger Ltd., Bristol, Great Britain, 1986.

[9] Wikipedia, Anti-reflective Coating, Online reference: http://en.wikipedia.org/wiki/Anti-reflective_coating, sighted on 18/06/2010, pp-4.

[10] C. E. Valdivia et al., "Optimization of antireflection coating design for multi-junction solar cells and concentrator systems", Proceedings of the Society of Photo-Optical Instrumentation Engineers vol 7099, 2008.

[11] M. F. Schubert et al., "Design of multilayer antireflection coatings made from

co-sputtered and low-refractive-index materials by genetic algorithm.", pp. 5290-5298, Optics Express Vol 16, Issue 8,2008.

[12] M. Autotype, "Novel film inspired by moths", Autoflex MARAG, The Engineers Supplier's Network, 2003. www.engineeringtalk.com/news/aue/aue124.html.

[13] Y. T. Lee, "High-efficiency GaInP/LCM-GaInP/GaAs triple-junction solar cells with antireflective subwavelength structures", Gwangju Institute of Science & Technology (GIST), Korea, October 2009.

[14] M. Berger, "Moth eyes inspire self-cleaning antireflection nanotechnology coatings", Nano Werk Nanotechnology spotlight, 2008. http://www.nanowerk.com/spotlight/spotid=7938.php.

[15] M. A. Green, "Very high efficiency silicon solar cells - science and technology", Electron Devices, IEEE Transactions. Vol 46 Issue 10, pp. 1940-1947, 2002.

[16] C. N. R. Rao and A. K. Cheetham," Material Science at the Nanoscale", Chapter 1, Nanomaterial handbook.

[17] R. D. Glovert, J. M. Miller, and J. E. Hutchison, "Generation of Metal Nanoparticles from Silver and Copper Objects: Nanoparticle Dynamics on Surfaces and Potential Sources of Nanoparticles in the Environment", ACS nano, 5(11) pp. 8950-8957, ACS Publications, 2011.

[18] M. Ahmed , M.S. Alsalhi , M. K. J. Siddiqui "Silver Naoparticles Applications and Human Health", Clinica Chimica Acta, Volume 411, Pages 1841-1848, International Journal of Clinical Chemistry and Diagnostic Laboratory Medicine, 2010.

[19] Y. Qin, "Silver-containing alginate fibres and dressings", International Wound Journal Volume 2, pp. 172-176, June 2005.

[20] "Finite Difference Time Domain Photonics Simulation Software," OptiFDTD Technical background and Tutorials. Version 8.

[21] P. Silverman, "X-ray lithography: Status, challenges, and outlook for 0.13 mm," J. Vac. Sci. Tech. B, 15 (6), pp. 2117-2124, 1997.

[22] H. W. Deckman and J. H. Dunsmuir, "Applications of surface textures produced with natural lithography," J. Vac. Sci. Tech. B, **1** (4), p. 1109, 1983.

[23] M. N. Alam "High Performance Magneto-Optic Garnet Materials for Integrated Optics and Photonics" , PhD. Thesis, chapter 3, Edith Cowan

University, Perth, Australia, 2012.

[24] L. H. Van Vlack, “Elements of materials Science and Engineering”, Addition-Wesley, p. 134, 1985.

[25] J. D. Verhoeven “Fundamentals of physical Metallurgy”, Wiley, p. 326, New York, 1975.

[26] N. A. Brunelli, R. C. Flagan and K. P. Giaps, “Radial Differential Mobility Analyzer for One Nanometer Particle Classification”, Aerosol Science and Technology 43:1, pp.53-59, 2008.

[27] C. Englert B., “Nanomaterials and the environment: uses, methods and measurement.” J. Environ Monit, 9(11), pp.1154-1161, Nov. 2007.

[28] T. P. Burg, M. Godin, S. M. Knudsen, W. Shen, G. Carlson, J. S. Foster, K. Babcock and S R. Manalis, “Weighing of biomolecules, single cells and single nanoparticles in fluid”, Nature 446, 1066-1069, April 2007.

[29] D. J. Burleson, M. D Driessen. & R.L Penn, “On the Characterization of Environmental nanoparticles”, Journal. of Environment Science & Health, A39(10), pp.2707-2753, 2004.

[30] E. Hontanon. And F. E. Kruis, “A differential Mobility Analyzer (DMA) for Size Selection of Nanoparticles at high flow rates”, Aerosol Science and Technology 43:1, pp.25-37, 2009.

[31] F. Tiago and R. Wayne, “The ImageJ User Guide 1.44” February, 2011.

[32] Y. M. Song, “Design, Fabrication and Characterization of Antireflective Subwavelength Structures (SWSs) for Optical Device Applications”, PhD. Thesis, Gwangju Institute of Science and Technology, pp. 36, 2010.